An integrated sedimentological, rock typing, image logs, and artificial neural networks analysis for reservoir quality assessment of the heterogeneous fluvial-deltaic Messinian Abu Madi reservoirs, Salma Field, onshore East Nile Delta, Egypt

Nader H. El-Gendy[1], Ahmed E. Radwan[2]*, Mohamed A. Waziry[3], ***Thomas J.H. Dodd[4], and*** **Moataz Kh. Barakat[1]**

[1]Geology Department, Faculty of Science, Tanta University, Tanta 31527, Egypt

[2]Faculty of Geography and Geology, Institute of Geological Sciences, Jagiellonian University, Gronostajowa 3a; 30-387 Kraków, Poland

[3]Dana Gas Company, New Cairo, Egypt

[4]British Geological Survey, Lyell Center, Research Avenue South, Edinburgh, EH21 6ER

*Corresponding author, e-mail: radwanae@yahoo.com; ahmed.radwan@uj.edu.pl

Abstract

This study introduces an integrated evaluation of geological and geophysical data, including sedimentology, diagenetic alteration, image log analysis, core measurements, formation evaluation, and a neural analysis technique (K-mode algorithm) to characterize the upper Messinian heterogeneous reservoirs of the Salma Field, Nile Delta, Egypt. It links observed reservoir permeability and flow zone indicators (FZI) to predict reservoir quality and distribution within un-cored parts of the field. Core and image log analysis show that the Abu Madi sandstone reservoir is composed of seven clastic litho-facies deposited within fluvial to deltaic environments. The reservoir is controlled by four hydraulic flow units (HFU's) and five flow units (FU). Fluvial channel facies, tidally influenced fluvial channel facies, and uppermost parts of bayhead delta facies are dominated by clean sandstone with a low clay content (avg. 20%). These facies are characterized by the high pore-throat sizes (R35 and FZI values), indicating a pore system dominated by mega- to macro-pores. The estuarine facies is composed of mudstone, siltstone, and argillaceous sandstone, with 25% average clay content and moderate R35 and FZI values, indicating a pore system dominated by macro- to meso-pores. The heterolithic estuarine and bayhead delta facies contain abundant argillaceous-rich sandstones, with 29% average clay content and low R35 and FZI values, indicating a pore system dominated by micro-pores. A neural log technique was applied to predict FZIs and permeability in un-cored intervals. Paleocurrent analysis was conducted using image log data to guide sweet spot and reservoir quality tracking across the field. Reservoir quality is controlled by both diagenetic and depositional processes, chiefly an abundance of detrital clays, grain size, and sorting. In the Salama Field reservoirs, mineral dissolution, cement dissolution, and micro-fractures enhance the pore system, while pore-filling and grain-coating detrital clays reduce reservoir quality. These results are important as they improve the wider understanding of the Messinian Abu Madi reservoir in the wider Mediterranean region.

Keywords

Fluvio-deltaic; reservoir quality; neural analysis techniques; rock typing; Salma Field; Messinian Nile Delta

1. Introduction

This study evaluates the Upper Messinian reservoir rocks and in-particular the Abu Madi reservoirs of the Salma Field. The Abu Madi sandstone is the main gas-producing formation from the Salma Field in the East Nile Delta region (Fig. 1). The Upper Messinian succession is considered the main hydrocarbon reservoir interval that contains substantial gas reserves within the Nile Delta area, with a number of fields currently in production (EGPC, 1994; Barakat et al., 2021). The Upper Messinian has variable sedimentary lithofacies as a result of deposition in a range of different environments through time (EGPC, 1994; Dolson et al., 2005; Leila et al., 2015). During the late Miocene to early Pliocene, an entrenched valley system was filled with mainly sandstones (Leila & Moscariello, 2019), which were deposited during a series of fluctuation in relative sea level (EGPC, 1994; Dolson et al., 2001; Salem et al., 2005). The marine influence on deposition during Abu Madi times became stronger towards the end Miocene (Palmieri et al., 1996; Dalla et al., 1997), which resulted in the deposition of thick marine mudstones in-between sandstone bodies (Dolson et al., 2001).

The primary goal of reservoir evaluation is to characterize reservoir units and understand their relevant geology and reservoir properties, which is one of the key challenges in developing a reservoir model (Novak et al., 2014; Ali et al., 2021; Radwan, 2022a, b). Various methods were developed for consistent interpretation of available data to describe reservoir properties of the zone of interest in wells (Ezekwe & Filler, 2005), as well as prediction of petrophysical parameters throughout a reservoir using geostatistical and classical methods (Maschio et al., 2008; Demyanov et al., 2015; Abdullah et al., 2021a). Petrophysical parameters such as porosity and permeability are common aspects of fluid flow modeling (Corbett, 2009; Heidari et al., 2012; Mirzaei-Paiaman et al., 2018; Abdullah et al., 2021b). The significance of property modelling for petrophysical parameters and facies distribution characterization relevant to flow performance has been widely investigated (e.g., Corbett and Jensen, 1992; Jensen et al., 2000; Corbett, 2009; Soleimani and JodeiriShokri, 2015; Ghandra et al., 2015; Corbett and Duarte, 2019; Radwan et al., 2021b; Radwan, 2022a, b).

The quality of petroleum reservoirs is determined by their storage volume and flow capacity, which are intrinsically related to pore type and size distribution (e.g., Corbett, 2009; Taylor et al., 2010). Calculating accurate hydrocarbon reserves is often challenging, largely due to reservoir facies variability and its impact on reservoir parameters, which ultimately effects the total available pore hydrocarbon volume.

The reservoir environment and depositional processes have an impact on the pore system in petroleum reservoirs (Soleimani et al., 2017; Radwan, 2021; Radwan et al., 2021a, c). Petrophysical properties of the reservoir are best-informed by an in-depth understanding of sedimentary process of emplacement and overall depositional setting. Reservoir diagenesis plays a critical role in the improvement and/or reduction of reservoir quality (e.g., Ajdukiewicz and Lander, 2010; Taylor et al., 2010). Integrated reservoir characterization using a variety of datasets is essential in the evaluation of static and dynamic properties (Jones et al., 2009; Radwan, 2022).

Reservoir rock-typing is the main process for reservoir classification into flow units (Mirzaei-Paiaman et al., 2018; Nabawy et al., 2018a; Radwan et al., 2021b). Analysis techniques that can be combined to determine reservoir flow unit parameters include core analysis, image log analysis, and log data analysis (Beiranvand & Kamali, 2004; Al-Ibadi & Al-Jawad, 2020; Radwan et al., 2021). Rock-typing is an integrated multi-proxy approach for reservoir characterization and field production optimization that employs geological, petrophysical, and engineering data to better-characterize heterogenous reservoir units and define their potential performance (Guo et al., 2005; Gomes et al., 2008; Al-Farisi et al., 2009; Masalmeh et al., 2012; Skalinski & Kenter, 2014; Nabawy et al., 2018b; Radwan et al., 2021; Barakat, 2022; Nabawy et al., 2022a,b). Most advanced rock typing techniques, such as the 'Winland's R35' method (Pittman, 1992), the reservoir quality index (RQI) determination (Leverett, 1941), and the flow zone indicator (FZI) calculation for flow unit identification, rely on data from core measurements (e.g., Amaefule et al., 1993; El-Sharawya et al., 2020; El-Adl et al., 2021).

There is a general lack of core data through the key reservoir section within the Salama Field, and so accurate lithological and reservoir parameter information has limited the understanding of the pore system. This integrated study combines a comprehensive evaluation and characterization of geological and petrophysical datasets, including analysis of sedimentary facies, diagenetic alteration, image data covering non-cored intervals, core data, petrophysical evaluation of well-logs, and artificial neural analysis techniques to better understand the reservoir characteristics. The application of artificial neural analysis techniques to the wider well dataset may provide an appropriate solution to aid the prediction of petrophysical parameters within the reservoir, especially in non-cored intervals.

Through this analysis, this study 1) examines and characterizes the lithofacies and their dynamic flow results to improve estimates of reservoir flow units within the Abu Madi sandstone; 2) constructs a depositional model for the Abu Madi sandstone reservoir using core and image log data; 3) explores the effects of diagenesis on reservoir quality; and 4) applies an artificial neural analysis technique for predicting the FZI and permeability distribution of un-cored intervals. The results of this study have basin-scale implications in terms of improved hydrocarbon reservoir understanding in the East Nile Delta region, and more-widely through the characterization of the Messinian sedimentology, stratigraphy, and reservoir quality in the Mediterranean region.

2. Geological setting

In the Nile Delta and the Mediterranean, hydrocarbon reservoirs in the onshore region are formed by Neogene-Quaternary siliciclastic sequences (Fig. 2; EGPC, 1994; Leila et al., 2022a). The Messinian section, including the Qawasim and Abu Madi formations, hosts the most economically important potential reservoirs in the Nile Delta (EGPC, 1994; El-Nikhely et al., 2022). The Abu-Madi Baltim trend in West El Manzala has been described as a series of backstepping fluvial channels (Palmieri et al., 1996; Dolson et al., 2005; Abdel-Fattah and Slatt, 2013). This backstepping was formed by transgressions that reached further south over time, finally resulting in the major transgression that gave rise to the deposition of the Kafr El Sheikh Formation (EGPC, 1994; Abdel-Fattah and Slatt, 2013). During transgression, the deposited sediments were shifted south into the eroded valleys, closer to the sediment source (EGPC, 1994). The dramatic fluctuations in relative sea-level, both during and after the Messinian salinity crisis formed the deeply incised valley of the Eonile Canyon (EGPC, 1994; Abdel-Fattah and Slatt, 2013; Leila and Moscariello, 2019). The Eonile Canyon was infilled by deposits of the Messinian salinity crisis and was covered by a thick pile of Pliocene-Pleistocene sediments (EGPC, 1994). The large Eonile Canyon forms in both modern-day onshore and offshore areas (Barber, 1981; Dalla et al., 1997; Dolson et al., 2001; Barakat et al., 2019). Extensive areas outside the incised canyon were subjected to erosion during low sea-level periods, and experienced sediment aggradation during initial period of transgression (EGPC, 1994). Marine clays were deposited when the transgression reached its peak. Figure 2 shows the tectonostratigraphic framework of the Nile Delta and the Mediterranean, with hydrocarbon reservoirs in the onshore region represented by Neogene-Quaternary siliciclastic sequences (EGPC, 1994; Leila et al., 2022a). The Messinian section, including the Qawasim and Abu Madi formations, hosts the most economically important potential reservoirs in the Nile Delta.

Messinian depositional trends were affected by Miocene faults, as well as older fault trends. The base Messinian surface is more affected by older faults, whilst the younger Messinian being influenced by reactivated Miocene faults (Fig. 3). This resulted in Messinian depositional trends that vary from the north-west to the south-east at the base, and from broadly north to south at the top. The highest area in the east of the Nile Delta today is in the southernmost part, which represents a north-west dipping paleo-high structure that has existed since the Messinian (Fig. 3). This paleo high controlled the thickness and palaeo-flow direction of the Messinian sedimentary pile (Yehia et al., 2019). Deep faults crosscut the crest of the structure, and form potential vertical hydrocarbon migration pathways into available traps (EGPC, 1994; Abdel-Fattah and Slatt, 2013; Leila and Moscariello, 2019).

Within the area of the Salma Field, the Abu Madi Formation is interpreted as deposits of a broad fluvial channel system, aligned roughly parallel to the gas-producing system of the Abu Madi to the west (Leila et al., 2022b). The Abu Madi Formation is sub-divided into two units in the Nile Delta region, including the upper Abu Madi unit and lower Abu Madi unit; the upper Abu Madi unit is absent within the Salma Field.

3. Methodology

All available data were used for the study of the Salma Field, west of the Qantara concession, Nile Delta, Egypt (Fig. 1). This included information from two key wells: Salma 2 and Salma 4, which are from within the Salma Field. A complete set of well logs were available, including core petrography, thin sections, and formation micro image logs (FMI) for both the Salma-4 and Salma-2 wells; only core analysis data was available for the Salma-2 well. For this study, Techlog™ (Version 2015) from Schlumberger Inc. was utilized for log data evaluation.

3.1 Core petrography

The uppermost part of the Abu Madi Formation reservoir is intersected in the two wells. The petrographical study was carried out on 25 thin sections that were prepared using selected core samples from the Salma-4 well. Thin section preparation included the injection of blue dye resin to enable porosity identification, and staining by a solution of Alizarin Red-S and potassium ferricyanide mixture to enable carbonate mineral identification. In addition, samples were stained with a solution of sodium cobalt nitrate to aid in the identification of alkali feldspar (*sensu* Tucker, 1988). Thin sections were examined under a polarizing microscope to study mineral composition and texture. Sandstones were classified according to the modified version of the sandstone classification scheme, as described by Dott (1964). For each thin section, the mineralogy, texture, and pinpoint porosity were defined. The relative abundances of authigenic and detrital components were calculated in percentage (%) by volume. Porosity was determined using a point counting technique (200 points for each sample).

3.2 Borehole image logs

Borehole image logs provide high-resolution information to visualize sedimentary structures, facies types, geomechanical characteristics, and depositional trends (Lai et al., 2018; Hassan et al., 2022). Significant advancements in imaging technology have been made, especially in its application to non-cored intervals (Lai et al., 2018; Hassan et al., 2022).

Core image data was available for 49 m of the Salma-2 well, and 41 m for the Salma-4 well. The core image data were used for sedimentary logging, facies description, and depositional environment interpretation. Image log (FMI) data from both cored and non-cored intervals were used to evaluate lithofacies, depositional elements, and paleo-current direction (*sensu* Tucker, 2001; Donselaar and Schmidt, 2005; Folkestad et al., 2012; Miall, 2014; Lai et al., 2018; Hassan et al., 2022). The interpretation of borehole imaging data from the studied wells followed the modern standard techniques in the oil and gas industry (e.g., Lagraba et al., 2010; Lai et al., 2018; Hassan et al., 2022).

3.3 Core analysis

Core analysis was performed at the Corex Laboratory in Egypt. Grain density, porosity, and permeability were measured from 58 conventional core plugs taken from the Salma-2 well and 90 conventional core plugs in the Salma-4 well. Special core analysis (SCAL) was completed on 23 core plugs from the Salma-2 well and 56 plugs from Salma-4. Analysis included electric reservoir properties such as Archie exponents (a, m, n), porosity and permeability under overburden pressure, and fluid mercury injection for pore throat and capillary pressure tests (MICP). A gamma-ray correction of the core depth with respect to log depth was conducted. Porosity and permeability data were corrected to net overburden pressure at reservoir conditions to achieve in-situ values (Dubois et al., 2006).

This study applies various methodologies to distinguish between different flow units within the Abu Madi Formation reservoir. Rock typing is used for classifying reservoir facies into rock types based on their dynamic behavior (Varavur et al., 2005). The dynamic behavior depends on the diagenetic processes, textures, and fluid relationships within the rock mass (Bear, 1972; Gomes et al., 2008). Semi-empirical equations can be applied to optimize rock permeability determination under various loading conditions (Panda and Lake, 1994; Bernabé et al., 2003; Costa, 2006; El -Gendy et al., 2020). Winland (1972) constructed an empirical relationship to predict rock flow units (Tiab and Donaldson, 1996; Gunter et al., 1997). The porosity and uncorrected air permeability were measured using conventional analytical techniques, whilst pore throat radii were determined using mercury injection.

In the reservoir, the flow unit (R35) is defined according to a uniform pore throat size distribution and similar flow performance. The R35 Equations are provided below (1&2; Kolodzie, 1980; Pittman, 1992).

$$\text{Log } R35 = 0.732 + 0.588 \log Ka - 0.864 \log \Phi \text{ core} \qquad (1)$$

$$R35 = 10 \wedge (0.732 + 0.588 \log Ka - 0.864 \log \Phi) \qquad (2)$$

Where: R35 is the radius of pore throat parallel to the 35% of mercury saturation,

Ka is uncorrected air permeability (in mD), and Φ is effective porosity in (%).

R35 indicates the inflection point when pore throat size is cross plotted against mercury saturation (Katz, 1986; Gunter et al., 1997).

The second approach is based on the reservoir quality index (RQI) (Leverett, 1941), and flow zone indicator (FZI) (Amaefule et al., 1993; Barakat and Nooh, 2017; Nabawy et al., 2020; Radwan et al., 2021b). Rock is classified according to RQI and flow properties (Amaefule et al., 1993; Nabawy and Barakat, 2017; Radwan et al., 2021b). The RQI equation is based on the theory that a porous medium can be represented by a package of capillary tubes (Kozeny, 1927), and permeability can be expressed as follows:

$$K = \frac{\emptyset}{8t} \; r2 \qquad (3)$$

Where K is permeability in μm^2, Ø is effective porosity infraction, r is the radius of the capillary tubes and t is tortuosity.

Carmen, (1937) modified Equation 1 into the 'Kozeny-Carmen' model with the following generalized form:

$$K = \left(1/_{fs.t^2.\ S^2gv} \right) * \ \emptyset^3/_{(1-\emptyset)^2} \qquad (4)$$

Where fs is shape factor and S^2gv is specific surface area for the grain volume unit in µm.

Amaefule et al. (1993) addressed the variables of the Kozeny constant and S2 characteristics of porous media.

$$FZI = 1/\sqrt{fs.t \wedge 2.\ S^2gv} \qquad (5)$$

$$K = {Ø^3}/{(1-Ø)^2} * FZI^2 \quad (6)$$

$$\sqrt{K}/Ø = [Ø / (1-Ø)] * FZI \quad (7)$$

Where permeability is expressed in mD, and RQI (µm) is written as:

$$RQI = 0.0314\sqrt{K/Ø} \quad (8)$$

The hydraulic flow concept is used to divide a reservoir into units with unique FZI values (Al-Ajmi & Holditch, 2000). The FZI approach combines petrophysical data with environmental factors to classify the reservoir into different hydraulic flow units (HFUs), which are defined as a representative reservoir volume with almost identical petrophysical and fluid properties (Amaefule et al., 1993). FZI was calculated using RQI and normalized porosity after applying the correction for porosity and permeability related to reservoir conditions. HFU's were defined from the FZI normal distribution values with the cumulative FZI curve, where the change in the slope of the cumulative curve represents a change in flow unit at the inflection point. The HFU in a reservoir is calculated from FZI and RQI (Amaefule et al., 1993; Guo et al., 2005).

$$FZI = {RQI}/{Øz} \quad (9)$$

$$Øz = {Ø}/{(1-Ø)} \quad (10)$$

Where Øz is the normalized porosity.

3.4 Well logs analysis

All available wells for Salma Field were used for petrophysical analysis (clay content, porosity, lithology, and fluid saturations). A quantitative evaluation of the muddy sandstone reservoir requires an accurate estimation of the clay volume (VSH). The gamma-ray indicator was used in the clay content calculation. The density-neutron and photoelectric curve (Pef) were used for lithology identification (Radwan et al., 2020). Effective porosity (PHIE) was computed from the neutron-density endpoint matrix cross-plot (Bateman, 1985) and corrected for VSH and gas effects. The lithology and grain density from the core data were used in the evaluation. The 'Indonesian Model' was applied (Poupon and Leveaux, 1971;

Archie, 1942; Bhatt et al., 2001) to determine the reservoir water saturation volume in the muddy sandstone formations. This assumed that formation waters are relatively fresh (salinity = 20,000 NaCl equivalent) and there is a high mudstone content. The cementation factor (m) and saturation index (n) were estimated from SCAL. The formation water resistivity (Rw) was calculated using a reservoir water production sample.

3.5 Neural log analysis

Petrophysical analysis and reservoir character attributes form as 1-D datasets within the borehole, and it is challenging to predict how they vary away from wells (Lucia, 2007; El-Gendy, 2017). Simulation-based methods are often applied to consistently identify rock types in sedimentary well logs (Gandhi et al., 2010; Heidari et al., 2011). To further aid this prediction away from the well bore, artificial neural networks have been applied to rock type classification and flow unit identification. Artificial neural network (ANN) techniques are important for well logging prediction (Dubois et al., 2006). ANN can be used to investigate the relationship between linear or non-linear input-output patterns, to generalize training groups, and estimate test groups. The neural log technique (K-mode) used in this study applies powerful neural network capabilities to predict poor or un-recorded data/parameters (e.g., 'K'). FZI data obtained from core tests and logging curves are used as training data for the FZI prediction in non-cored intervals. Using 'TechlogTM' software (K-mode), a statistical model using petrophysical parameters from well logs, and FZI from core measurements, was developed to predict the FZI curves on a log basis within cored intervals. Subsequently, this methodology was applied to un-cored intervals to gain additional information about those reservoir units. To create and develop a neural network model, input and training data are used, including input parameters (VSH, PHIE, Pef, and FZI), followed by application data, which will be used in the final prediction of required data (VSH, PHIE, and Pef).

3.6 Stratigraphic modified Lorenz plot (SMLP)

This graphical technique is the most effective for evaluating and separating the reservoir into distinguishable flow units (Tiab and Donaldson, 1996; Gunter et al., 1997), as well as assessing how each unit contributes to reservoir performance (Chopra et al., 1998; Gomes et al., 2008). Stratigraphic modified Lorenz plots (SMLP) are constructed by plotting flow capacity (%Kh) versus storage capacity (%Φh), where h is sample interval thickness, and k is permeability (mD). The partial sums are computed and normalized to 100%, then arranged in stratigraphic order (Gomes et al., 2008). Gradients with steep angles represent a higher flow capacity in relation to unit storage capacity, which are often referred to as 'speed zones' (Chopra et al., 1998). Intervals with low storage capacity and minor flow capacity typically form baffles to flow within the reservoir. Finally, intervals with no flow or storage capacity are regarded as sealing units (Salazar, 2006; Gunter et al., 1997).

4. Results

4.1 Core and image log interpretation

The core data and image log were interpreted for contained lithofacies, depositional elements, and overall environment of deposition. The reservoir interval within the Salma-2 and Salma-4 wells was divided into the lower, middle, and upper units, which are characterized by seven facies.

4.1.1 Sub-aerial gravity-flow facies

The sedimentary facies of the basal zone consist of deformed mudstone and mixed mudstone and sandstone heterolithic deposits. These sedimentary rocks display erosional basal contacts (see incision facies C in Fig. 4) and form repeated successions.

It is interpreted that these deposits represent sub-aerial gravity-flow facies, which were accumulated directly after the scour of the canyon, and formed through the de-stabilization of the canyon walls. Other evidence of valley bank collapse accompanying local collapses and mudslides during within this interval have been observed elsewhere (*sensu* Blair and McPherson, 1994; Hunger et al., 2001). However, It is also possible that these mudslides formed through a complex sequence of erosion, iso-static distortion, sea-level drop, and water release processes that occurred during the Messinian Salinity Crisis (MSC) (Gargani et al., 2010).

4.1.2 Fluvial channel facies

The fluvial channel facies represent the majority of the Abu Madi basal reservoir unit. It is composed of blocky massive coarse-grained sandstones, and occasional conglomeratic sandstones, with sharp and erosional contacts that represent the scour surface at the base of this facies. The sandstone is poorly-sorted at the base, becoming moderately-sorted towards the top, where an overall fining-upward trend is observed. Massive kaolinitic pebbly sandstones (Fig. 4) are interpreted as being deposited rapidly, during a high-energy flow event. The lack of interbedded mud-drapes or mudstone beds supports a period of high hydrodynamic energy.

The multiple amalgamated scour surfaces filled with coarse-grained poorly-sorted and moderately-sorted sandstones, as well as the distinct lack of intervening mudstone units, indicates the presence of stacked fluvial channel elements (Bridge, 2006). The presence of sandstone beneath and overlying horizontal laminations of very light brown colored mudstone, as well as the absence of any bioturbation or ichnofossils, suggests a high energy fluvial channel formed in a terrestrial setting (Miall, 1977; Tucker, 2001).

4.1.3 Tidal channel facies

This tidal channel facies consists of lowermost beds of poorly-sorted coarse-grained massive (or structureless) sandstones with sharp-bases, and a fining-upwards succession of moderate- to well-sorted sandstones (Fig. 5). The sandstones are characterized by parallel lamination and trough cross-bedding, ripple-cross lamination, upwards increasing bioturbation, an upward increase of mud-drapes, and glauconite.

The normally graded sandstones with trough cross bedding, followed by parallel lamination and/or ripple cross bedding, is interpreted as representing in-channel deposition. The fine-grained glauconitic sediments and mud-drapes at the top of these deposits indicate the influence of shallow waters and tidal currents (Terwindt, 1971; Van den Berg, 2007). The upwards increase in bioturbation can be used to infer a transition from brackish to freshwater conditions (MacEachern and Bann, 2008).

4.1.4 Tidal flat facies

The tidal flat facies are composed of grey laminated mudstones, siltstones, and occasionally very fine-grained lenticular sandstones. Low-angle to horizontal laminations and mud-drapes form wavy bedded heterolithic units, which contain abundant bioturbation and rhizoliths (Figs 4A and 5D).

These facies are interpreted to have formed in a restricted tidal flat environment. The presence of lenticular beds, mud-drapes, and wavy bedding can be used to indicate a complex mixture of higher energy oscillatory wave action, and intermittent periods of lower energy sedimentary processes, which together suggests a component of tidally-influence on sedimentation (Klein, 1971; Buatois, 1999). The presence of abundant bioturbation, and importantly the development of rhizoliths, indicates a very shallow water setting, certainly where parts were exposed for prolonged periods, during which time roots were able to establish within the substrate.

4.1.5 Tidally influenced fluvial channel facies

The tidally influenced fluvial channel facies are composed of brown moderately-sorted, occasionally poorly-sorted, coarse- to very coarse-grained, massive (structureless), pebbly or kaolinitic sandstone. The basal part comprises brown sandstone with intercalated multi-colored mudstones (Fig. 5). An overall fining-upwards is recognized within this unit, with sediments becoming fine-grained and moderately-sorted towards the top. Parallel laminations and abundant mud-drapes are recognized throughout, and glauconite plus flame structures are present near to the top. The fine-grained sandstones typically display wave ripple-cross lamination, cross-stratification, wavy bedding, flaser lamination, and abundant reactivation surfaces (Fig. 5).

The erosive-bases and fining-upward trend may be used to indicate deposition in a tidally influenced channel (Terwindt, 1971), whilst multiple stacked erosion surfaces, which form an amalgamated succession, suggest the presence of multiple stacked channels (*sensu* Van den berg et al., 2007). The presence of massive pebbly sandstones at the base and flame structures at the top suggests rapid deposition under a high hydrodynamic regime. Multi-colored mudstones and glauconite suggests complex reducing conditions, which is normally-indicative of a restricted shallow water environment. The abundance of flaser lamination/bedding, wavy bedding, abundant reactivation surfaces, and mud-drapes strongly suggest tidal influence on sedimentation.

4.1.6 Flood plain facies

The flood plain facies consists of light grey siltstones and poorly- to moderately-sorted very fine-grained glauconitic and bioclastic sandstones and interbedded mudstones (Fig. 5). Sandstones display both symmetrical and asymmetrical ripple cross-lamination, tidal bundles, and mud-draped reactivation surfaces, the latter being more common near the top of the succession.

The light grey mudstones and siltstones reflect well-drained proximal floodplain deposition in a hydrodynamically low-energy setting. Evidence for intermittent tidal influence on sedimentation is provided by interbedded sandstones, with tidal bundles, glauconite, symmetrical ripple cross-lamination, and mud-draped reactivation surfaces, which are interpreted to reflect the deposits of a progressive transgression of the shelf.

4.1.7 Sabkha facies

The sabkha facies comprises multi-colored laminated mudstones with very brittle and indurated surfaces (indicating sub-aerial exposure), bioturbated siltstones, and occasion muddy-sandstone interbeds. Anhydrite is observed formed as nodules within the argillaceous matrix (Fig. 5). An upwards increase in evaporite textures occurs, which is succeeded by a thick anhydrite bed.

This facies reflects a low-energy restricted shallow water environment, most likely within a sub-tidal lagoon setting. Anhydrite nodules were formed during periods of sub-aerial exposure (Kinsman, 1969). The bioturbated siltstones and muddy-sandstones interbeds are interpreted to have been deposited during semi-arid periods. Importantly, and largely because of the bedded anhydrite, this facies represents a non-permeable layer that may form a potential intra-reservoir barrier to fluid flow.

4.2 Facies characteristics of the Abu Madi reservoir

Detailed thin section (TS) analysis allowed the identification and characterization of the detrital and authigenic components of the Abu Madi reservoir. Relative abundances of components (% by volume) were obtained through point counting on thin sections (200 points for each TS). The analyzed sandstone samples from the Salma-4 well include sub-feldspathic arenite (48%), sub-feldspathic wacke (28%), sub-lithic arenite (8%), feldspathic wacke (8%), anhydrite sub-feldspathic (4%), and lithic arenite (4%) (Fig. 6; after Dott, 1964).

The sabkha facies (Fig. 7A) contains mudstone and argillaceous matrix composed of anhydrite, sub-feldspathic arenite, and silt to coarse-grained sand. It is moderate- to well-sorted, rounded- to sub-angular, moderately cemented, and occasionally highly cemented. Frequent monocrystalline quartz grains (Qz) occur, as well as K-feldspars (K) and traces of mica flakes. Opaque minerals and pore-filling anhydrite crystals (An) are observed. This facies displays poor to moderate pore interconnectivity.

The flood plain facies (Fig. 7B) comprises silt to coarse-grained sand, represented by sub-feldspathic arenite and wacke, which are poorly-cemented, moderately-compacted, and contain abundant monocrystalline quartz grains. Small amounts of K-feldspar, detrital glauconite pellets (G), bioclasts (B), and plagioclase feldspars (Ps) are present. The sandstone has moderate to good pore interconnectivity.

The tidally influenced fluvial channel facies is composed of mainly fine- to coarse-grained sand (Fig. 7C) that can be classified as a sub-feldspathic arenite. These rock units are dominated by quartz grains that are moderate- to well-sorted, rounded to sub-angular, poorly cemented, and moderately compacted. It contains small amounts of K-feldspars, bioclasts, and rare amounts of heavy minerals and opaques (see green arrows on Fig. 7). The sandstones of this facies have good pore interconnectivity.

The fluvial channel facies can be classified as a sub-lithic arenite (Fig. 7D). It is mainly composed of silt to granule grade material, the latter of which are typically poorly-sorted and sub-angular to rounded. The sandstones are poorly-cemented and moderately-compacted, with common pore-filling and grain-coating detrital clays (Dc), as well as small amounts of bioclasts (B) and shell fragments. The sandstones of this facies have moderate to good pore interconnectivity.

The tidal flat sedimentary facies are composed of very fine-grained sandstones and siltstones (Fig. 7E). The moderately sorted- to well-sorted, rounded to sub-angular sandstone, which are poorly-cemented and weakly compacted, can be classified as a sub-feldspathic wacke. The sandstones contain frequent examples of pore-filling and grain-coating detrital authigenic clays (Dc), as well as small amounts of K-feldspars. The sandstones of this facies have poor pore interconnectivity.

The tidal channel facies (Fig. 7F) is represented by sub-feldspathic arenites and wackes. The sandstones are poorly- to moderately-sorted, rounded to sub-angular, poorly cemented, and moderately compacted, with small amounts of K-feldspar. The sandstones of this facies have moderate pore interconnectivity.

4.3 Diagenetic features

The Abu Madi sandstone samples show multiple diagenetic features, including dissolution, fracturing, cementation, and compaction, which all play a role in the development of the final pore network. Diagenetic features related to fracturing were also recorded, which when present can act to enhance reservoir characteristics (Figs 7E, 7F). Grains show evidence for moderate compaction and associated microfractures resulting from grain-to-grain point contacts (Fig. 7). Cementation by micro and pseudo sparite was observed in TS, particularly where detrital clays were dominant (Figs 7A, 7B, 7E, 7F). Anhydrite cementation is dominant in the heterolithic sandstones (Fig. 7A), which can act to block pore throats and reduce overall reservoir quality. The dissolution of cement and feldspars is recoded in a few samples (Figs 7E, 7B). Finally, in some cases residual hydrocarbons are observed filling pore spaces (i.e., pore spaces related to dissolution of the cements and feldspars) that were formed during the late stages of diagenesis (Fig. 7E).

4.4 FMI Image data analysis from non-cored intervals

The Abu Madi facies identification in non-cored intervals was completed using formation image data (FMI) from the Salma-4 well between 2080–2280 m MDBRT (Fig. 8). These logs were interpreted for lithology, sedimentological features, and sedimentary facies.

The lowermost unit between 2280–2180 m MDBRT is dominated by a repeated (cyclic) fining-upwards succession of coarse- to very coarse-grained pebbly sandstones that are massive or cross-stratified, with numerous scour surfaces. The dip data display average north-west dip azimuths associated with paleo-current indicators. This unit is interpreted as fluvial channel deposits.

The middle unit between 2180–2138 m MDBRT and 2125–2100 m MDBRT is composed of horizontally-stratified and massively-bedded units in the lower part, while the upper part comprises laminated muddy-sandstones, laminated siltstones, and heterolithic sediments, with a general fining upward pattern (Fig. 9). The presence of siltstone and mudstone interbeds indicates the periods of energy decrease and deposition from lower energy flows. Based on the observed lithofacies and dip data, the middle unit is interpreted as amalgamated tidal channel and tidal flat deposits.

The upper unit between 2100–2080 m MDBRT (Fig. 9B), is formed by alternating units of massively-bedded muddy sandstones with cross-stratified sandstones, which is especially clear near the top of the unit. The unit displays an overall coarsening-upward pattern. The dip data show an east to north-east dip azimuth. This unit is interpreted as deposits of a tidal bar in a bayhead delta setting. However, the very upper-most zone of this interval shows slightly divergent dip data relating to palaeocurrent direction, which trends in both north-east and north-west dip azimuth. It is interpreted that these palaeocurrent directions represent deposition within the original fluvial channel direction, but which are modified by the influence of a contrasting tide direction (Fig. 10).

4.5 Depositional model from image data

The Abu Madi facies sediments are represented by three key zones (Fig. 11): the upper, middle, and lower. The lower zone (A) represents a fluvial channel depositional environment (Fluvial Domain). It consists of sharp-based aggrading fluvial facies, with stacked fluvial channel-fill sediments, and finning-upward successions, which collectively represent an initial north-westerly directed progradational phase.

The middle zone represents a tidally-influenced marginal marine depositional environment with three internal sub-units represented by an estuary, delta progradation, and finally a return to estuarine conditions. The lower sub-unit is represented by an estuarine environment (B; estuarine domain) and formed through the deposition under low accommodation space corresponding to a retro-gradational phase and transition from terrestrial to marine sedimentation. The middle sub-unit reflects deposition in a bayhead delta setting (C; tidal domain), during which gradual cyclic progradation of the sediments under tidal action occurred. Beds show a progradational phase. The facies are primarily composed of sandstone, with sandy tidal flats formed on a bayhead delta plain, and heterolithic facies representing tidal influences in adjacent areas. The upper sub-unit marks a return to estuarine deposition (B; estuarine domain) following the progradation of the bayhead delta during middle sub-unit times.

The upper zone represents a tidal environment and consists of two sub-units. The lower-most sub-unit represents a tidally influenced fluvial channel system (D; tidal domain). It also displays a change in palaeocurrent direction, as indicated by north-east to north-west dip azimuths. The upper-most sub-unit is represented by Sabkha deposits (E; tidal domain), which formed in a supratidal setting. The Sabkha deposits contain intercalated and bedded anhydrite, as well as fine-grained tidal flat facies.

The facies and depositional model (Fig. 11) depicts initial deposition in a continental setting in which fluvial processes dominated. This was followed by an fining-upward pattern, with an erosive scouring possibly related to lowstand to transgressive system tract conditions. Continued and widespread transgression of the palaeoshelf occurred resulting in a switch to marginal-marine sedimentary processes. Initial deposits were formed in a tidally-dominated estuary, with subsequent phases of progradation forming fluvial-dominated deposits within a bayhead delta. Finally, the depositional environment transitioned into a restricted tidal flat setting and/or Sabkha associated with the early onset of highstand conditions.

4.6 Rock type classification and flow unit identification

Rock typing is a technique used for classifying the reservoir into units of unique petrophysical characteristics. It is used to establish the relationship between reservoir parameters from different sources, such as core data, logs, production data, and geological descriptions (Amaefule et al., 1993).

4.6.1 Winland's R_{35} and flow units (FU)

Flow units were distinguished from the porosity-air permeability plot of cored intervals of the Abu Madi Formation (Fig. 12). The results of the flow unit assessment are presented in table (1), based on the range of pore-throat radii (R35) to five flow units (FU's):

1. FU-I: A flow unit with a R35 value of above 15 µm, which can be classified as having mega-pores. The porosity range is 24–39 % and permeability is often >900 mD. FU-I directly relates to fluvial channel and tidally influenced fluvial channel facies within the reservoir. The sandstones are relatively clean, contain only small amounts of argillaceous material, and have excellent reservoir quality.

2. FU-II: A flow unit with a R35 value ranging from 6–15 µm, which can be classified as having macro to mega-pores. The porosity range is 20–32 % and the permeability is 150–900 mD. It relates to the fluvial channel facies and tidally influenced fluvial channel deposits, which form very good reservoir units.

3. FU- III: A flow unit with R35 values ranging from 3.5–6 µm, which can be classified as having macro-pores. The porosity ranges between 16–30 % and the permeability ranges between 50–150 mD. This unit represents the estuarine tidal channel facies and the tidally influenced fluvial channel facies, which form good-quality reservoir units.

4. FU- IV: A flow unit with a R35 value ranging from 2–3.5 µm, which can be classified as having meso-pores. The porosity range is 13–31 %, while the permeability is 10–60 mD, and therefore represents medium to low-quality reservoir units.

5. FU- V: A flow unit with a R35 ranging from 0.5–2 µm, which can be classified as having micro-porosity. The porosity range is 14–26%, and the permeability range is 0.8–10 mD. This unit represents fluvial channel and the tidal channel (estuarine) facies, which form low-quality reservoir units.

Table 1: Statistical variability of petrophysical properties associated with each flow unit, based on Winland's flow unit classification:

Flow unit	R35 (μm)	Pores type	Porosity (%)	Permeability (mD)	Reservoir quality
FU I	>15	Mega pores	24–39	>900	Excellent
FU II	6–15	Macro- to Mega pores	20–32	150–900	Very Good
FU III	3.5–6	Macro pores	16–30	50–150	Good
FU IV	2–3.5	Meso pores	13–31	10–60	Moderate
FU V	0.5–2	Micro pores	14–26	0.8–10	Low

4.6.2 Normalized cumulative reservoir quality index (NCRQI)

Rock typing classification is based on the (RQI) concept and dynamic flow properties. From corrected core data that considers the reservoir condition in terms of porosity and permeability. RQI is calculated and used to determine (NCRQI) for each data point as follows:

$$NCRQI = \frac{\sum_{x=1}^{i} \sqrt{\frac{Ki}{\emptyset i}}}{\sum_{x=1}^{n} \sqrt{\frac{Kn}{\emptyset n}}} \qquad (11)$$

Where n and i are the total numbers of data and number of data points at sequential steps of computation, respectively. NCRQI depth curves for Salma-2 and Salma-4 wells (Fig. 13) show that the slope change NCRQI curve represents the change in reservoir flow unit (Gomes et al., 2008). The slope of the curve represents the rate of change of NCRQI with depth, where a high rate represents both high reservoir quality and flow rate. The reservoir units are separated (graphically) into different flow units based on change of curve slope.

The reservoirs show high-quality in units 1 & 2 (Table 1). These units have the highest porosity and permeability and are associated with fluvial and tidally--influenced fluvial facies. Unit 3 represent the medium-quality unit and is related to tidal channel facies, while the low-quality unit 4 corresponds to the heterolithic and argillaceous sandstones.

4.6.3 Hydraulic flow units (HFU)

The core data of Salma-2 and Salma-4 wells (Fig. 14) show four main HFU’s controlling the Abu Madi reservoir performance for the cored intervals. The defined HFU’s and reservoir facies are described in (Fig. 15), and the final HFU results for the Abu Madi Formation are summarized in Table (2).

HFU-I: The average FZI is between 4.5–10 µm, which represent excellent sandstone reservoir quality. Porosity ranges between 25–33 % and permeability exceeds 900 mD. This unit is mainly composed of fluvial channel and tidally influenced fluvial channel facies.

HFU-II: The average FZI is between 1.7–4.5 µm, reflecting a good to very good quality sandstone. Porosity ranges between 17–33 %, and permeabilities are between 70–900 mD. This unit is mainly composed of fluvial channel, tidal influenced fluvial channel, and clean sandstones of the tidal channels.

HFU-III: The average FZI is between 0.6–1.7 µm, reflecting a moderate quality sandstone. Porosity ranges between 12–33% and permeability between 4–100 mD. This unit is mainly composed of tidal channel and tidal flat sandstones (estuarine), with argillaceous parts of the fluvial and tidal influenced fluvial channel.

HFU-IV: The average FZI is between 0.2–0.6 µm, reflecting a low-quality sandstone. Porosity ranges between 15–30% and permeability between 0.6– 8 mD. This unit is represented by heterolithic sandstones of tidal flat facies.

Table 2. HFU data for the Abu Madi Formation.

Hydraulic flow unit	FZI (µm)	Porosity (%)	Permeability (mD)	Reservoir quality
HFU I	4.5–10	2533	>900	Excellent
HFU II	1.7–4.5	17–33	70–1000	Good - Very good
HFU III	0.6–1.7	12–33	4–100	Moderate - Good
HFU IV	0.2–0.6	15–30	0.6–8	Low

4.7 Formation evaluation

The evaluation of well logs has been performed to determine the petrophysical properties of the Abu Madi reservoir using graphical and computational methods. Log evaluation using 'TechlogTM' (Version, 2015) has been applied to determine shale volume, effective porosity, lithology, and hydrocarbon saturation. A large proportion of the data within the neutron-density raw data cross-plots for Salma-2 and Salama-4 wells demonstrate conformance with the sandstone trendline (Figs 16 and 17). Some points plot closer to the limestone line, which is interpreted as reflecting the presence of carbonate cementing minerals. Other points plot concordantly along the dolomite line, where the deposits contain shale. Finally, a cluster of data points plot above the sandstone line, which is likely caused by the gas effect (*sensu* Radwan et al., 2020). The thicknesses of the gas-bearing zone (net pay) for the two wells and other petrophysical analysis parameters are summarized in table (3). The Salma-2 well (Fig. 18), shows that all of the sandstone reservoir intervals are above the gas-water contact within the pay zone.

The Abu Madi sandstone is characterized by excellent reservoir quality, with high porosity (average porosity of 22%), and low clay content (average shale volume of 19%). This is especially the case in the lower zones, which represent the coarse-grained sandstone of fluvial channel facies with water saturation ranges between (20–40%). The upper zone of the reservoir is composed of lower quality fluvial channel facies, where the sandstones are finer-grained, and the clay content is higher. The upper part of the reservoir is interpreted as tidal channel and tidal flat facies, comprising fine- to very fine-grained sandstone, with mudstone intercalations. The Salma-4 well interpretation (Fig. 19) shows very good reservoir quality, with gas-bearing zones above 2113.4 m and water zones below 2117.5 m. The main pay zones in the upper part of Abu Madi are within high porosity tidally influenced fluvial channel sandstones. A small part of the good quality (average porosity of 22%) tidal channel sandstone net pay zone is above the 'gas down to' (GDT) level. The rest of Abu Madi reservoir is below the gas zone, with bayhead delta and fluvial channel sandstones being 'water-wet'. In general, the upper part is characterized by very fine-grained and clay-grade tidal flat sediments, with an overall high clay content (average shale volume of 21%). Clay content reduces resistivity (+/-3 ohm.m), whilst increasing irreducible water saturation

(>40%) (Tiab and Donaldson, 1996). The estuarine zone shows evidence for calcareous cements within the bayhead delta facies, which are interpreted to be formed through secondary processes during diagenesis within the estuarine environment.

Table 3: Petrophysical analysis of net pay zones in the Abu Madi Formation.

Well	Zones	Top (m)	Bottom (m)	Gross thickness (m)	Net pay (m)	Av. shale volume (%)	Av. porosity (%)	Av. water saturation (%)
Salma-2	Estuarine	2014.7	2025.4	10.7	2.60	26.0	18	36
Salma-2	Fluvial	2025.4	2070.0	44.6	22.70	19.0	22	40
Salma-4	Sabkha	2080.0	2088.5	8.5	0.15	34.0	19	47
Salma-4	Tidally influenced fluvial channel	2088.5	2100.0	11.5	9.80	21.4	24	39
Salma-4	Estuarine	2100.0	2115.0	15	2.29	21.0	22	60

4.8 FZI and permeability prediction

The neural log technique (K-mode) is statistical in nature and uses 148 core points for input data (PHIE and FZI based on core analysis) to predict FZI, with HFU's based on log data (PHIE, Pef, and Vshale). Using both log and core data within the cored zones, the neural analysis method iteratively uses FZI as a function related to log data to predict a FZI curve for non-cored intervals.

Using permeability (K) as a function on porosity(Ø), and FZI (Eq. 12).

$$K = 1014\,\mathrm{FZI}^2 * \text{Ø}^3 / (1 - \text{Ø})^2 \qquad (12)$$

The result of neural analysis of predicted FZI neural-derived and permeability calculations are presented in table (4). Although HFU's are limited by different FZI ranges, each unit may contain a wide range of potentially overlapping porosity and permeability values. The FZI values, along with seismic attribute information and sedimentary facies models, are used to define the character and distribution of flow units within the full reservoir model. The data from the core in Salma-2 and Salma-4 wells (Fig. 14) shows wide ranges of FZI across the main HFU's. Selected training data from cores covers most reservoir types and has been verified later with other cores. The resulting model provides an important tool for permeability prediction in reservoir flow simulation and production optimization.

In the Salma-2 well, FZI values are high within most reservoir intervals, including the un-cored sections dominated by flow units 1 and 2 (Figs 20 and 21), reflecting the high reservoir quality of fluvial channel sandstones. More minor intervals of the argillaceous fluvial channel flow unit 3 are also present. Permeability prediction shows a high permeability range in the lower zone, with a moderate range in other zones. The Salma-4 well contains alternating high and medium FZI values within the pay zone intervals, with medium-to-high permeability ranges. The middle part of the Abu Madi reservoir is below the gas zone (Fig. 21) and displays a low to moderate FZI range (flow units 3 and 2) in bayhead delta, estuarine, and tidal flat facies. The lower part of the Abu Madi reservoir is represented by a high range of FZI (flow unit 1), reflecting the variable sorting and coarser grain-sizes. The summary of HFU distribution for different reservoir units and environments is shown for Salma-2 (Fig. 22A) and Salma-4 (Fig. 22B).

Table 4: Petrophysical and neural analysis (FZI, Permeability) of reservoir zones for Abu Madi Formation.

Well	Zones	Gross thickness (m)	Net reservoir (m)	Av. shale volume (%)	Av. porosity (%)	Flow zone indicator (µm) Min - Max	Av. flow zone indicator (µm)	Av. horizontal permeability (mD)
Salma-2	Estuarine	10.7	2.6	26.0	18.0	1 – 7.2	3.9	356.7
Salma-2	Fluvial	44.6	22.9	19.0	22.0	1.8 – 7.0	4.5	648.3
Salma-4	Sabkha	8.5	0.3	29.6	17.3	0.5 – 2.0	1.8	24.7
Salma-4	Tidal influenced fluvial channel	11.5	9.8	21.4	24.0	1.8 – 8.5	3.7	676.7
Salma-4	Estuarine	66.9	10.7	25.0	18.9	1 – 9.0	2.2	173.4
Salma-4	Bayhead delta	13.9	10.4	24.6	18.3	1 – 6.0	1.9	83.1
Salma-4	Fluvial	94.4	64.9	21.0	19.7	1 – 10.6	3.5	683.9

4.9 Stratigraphic Modified Lorenz Plot (SMLP)

The cumulative percent of flow capacity (%Kh) was plotted versus the cumulative percent of storage capacity (%φh). Each slope segment represents the flow performance of a specific reservoir unit (Figs 23 and 24). The application of the 'Stratigraphic Modified Lorenz Plot' (SMLP) technique displays the main flow units, stratigraphically.

In Salma-2, flow performance is controlled by five units (A, B, C, D, and E; Fig. 23). The main units that contribute to the maximum storage and flow capacity are unit-A (45% storage and 40% flow) and unit-B (22% storage and 52% flow), which are fluvial channel facies in the middle and lower parts of the reservoir. The argillaceous fluvial channel deposits of units C and D in the upper part of the reservoir have low storage and flow capacity, whilst estuarine facies of unit E are sealing (7% storage and 6% flow).

In Salma-4, overall flow performance is controlled by 11 separate flow units (A–K; Fig. 24). The units that contribute the main storage and flow capacity are A, C, E, G, and J (35% storage and 86% flow, collectively), which are mostly related to tidally-influenced fluvial channel and estuarine facies of unit A. Unit E displays maximum flow performance (36%), which represents a 'speed zone', whilst flow units K and I represent low-quality reservoir intervals or baffles (22% storage and 4% flow, collectively). Units B, D, and F display very low-quality flow performance (20% storage and 1% flow) and considered as sealing units.

5. Discussion

5.1. Depositional and diagenetic controls on the reservoir quality

In general, fluvial deposits form highly heterogeneous reservoirs, where the connectivity of sand bodies and their characteristics control the reservoir quality at multiple scales (Gibling, 2006). In the study area, the Abu Madi Formation is composed of sabkha, fluvial channel, flood plain, tidally influenced fluvial channel, tidal flat, and tidal channel facies. This dynamic sedimentary system resulted in the deposition and preservation of variable sandstone types, including sub-feldspathic arenites, sub-feldspathic wackes, sub-lithic arenites, feldspathic wackes, anhydrite sub-feldspathic arenites, and lithic arenites. Each lithofacies has different characteristics and depositional conditions that control the texture, grain size, and sorting, which affect the reservoir quality. Additionally, diagenetic processes such as dissolution, fracturing, cementation, and compaction act to control the pore network in sandstone reservoirs (e.g., Worden and Burley, 2003; Taylor et al., 2010).

5.1.1 Sabkha Facies

The sandstones of the sabkha facies in Abu Madi reservoir (Figs. 5A and 7A) are dominated by anhydrite sub-feldspathic arenites, with argillaceous-rich silt grade to coarse-grained sandstones. Detrital clays within the matrix have a significant impact in terms of reducing reservoir quality, as do pore-filling anhydrite crystals (Fig. 7A), siderite bands, and anhydrite nodules, all features that can act to reduce overall porosity and permeability within the reservoir (*sensu* Elias et al., 2004). The grain contacts are dominated by point contacts, with only a few long concavo-convex contacts, which indicates low to moderate compaction. Overall, the sabkha facies sandstones in the Abu Madi reservoir are interpreted as poor to moderate in terms of reservoir quality (Fig. 7A).

5.1.2 Fluvial Channel Facies

The fluvial channel facies typically represent significant reservoir intervals, with high-quality porous and permeable sandstones often deposited and preserved in these settings (Mial, 1988; Luo et al., 2009; Morad et al., 2010; Leila et al., 2022a, b; Abdel-Fattah et al., 2022). The fluvial channel facies (Fig. 4B) are dominated by blocky and massively-bedded silt to granule grade poorly-sorted sandstones of the sub-lithic arenite type (Figs 4B and 7D), which show an overall fining-upwards trend. The massively bedded kaolinitic pebbly sandstones, along with the interbedded mudstone beds, absence of bioturbation, and mud-drapes, collectively suggest deposition in a fluvial channel setting (Allen, 1982; Mial, 1988; Bridge, 2006). The sandstones display a well-preserved primary porosity, with low amounts of pore filling and grain-coating detrital clays (Dc). The grains show only minor evidence of microfractures and grain contacts are dominated by point contacts, indicating a limited influence of compaction on reservoir quality (Fig 7D). The lateral continuity of correlated fluvial channel sandstones between the Salma-2 and Salma-4 wells is observed in the lower parts of the reservoir. In summary, the fluvial channel sandstone facies have very good pore interconnectivity, very good reservoir quality, and are more widely recognized as forming ideal intervals for gas storage and fluid flow (Allen, 1982; Mial, 1988; Bridge, 2006).

5.1.3 Flood Plain Facies

The flood plain facies (Fig. 7B) are dominated by silt to coarse-grained sub-feldspathic arenites. Grain contacts are dominated by point contacts, with a few long and concavo-convex contacts, reflecting low to moderate compaction. The grains are less compacted and have more space than compared with the sabkha facies. Thin section analysis shows scattered detrital clays that rare block pore spaces (Fig. 7B). Detrital clay abundance is less than compared with the sabkha facies (Fig. 7A) and the fluvial channel facies (Fig. 7D), which indicates higher porosity in the flood plain facies. Additionally, cementation by micro and pseudo sparite act to reduce the pore network, although porosity is observed to be fair to good. In summary, the flood plain facies have moderate to good pore interconnectivity and reservoir quality (Fig. 7B).

5.1.4 Tidally influenced Fluvial Channel Facies

The tidally influenced fluvial channel facies is a favorable reservoir in many petroleum systems worldwide (Hein, 2015). These facies are dominated by coarse-grained sub-feldspathic arenites (Fig. 7-C), with occasional gravelly-pebbly grains. Pore-filling kaolinite cements are observed (Fig. 5C). Grain contacts are dominated by point contacts, reflecting low to moderate compaction with visible preserved porosity (Fig. 7C). The commonly observed mud drapes are indicative of tidal influences on sedimentation (e.g., Allen, 1982; Martinius and Van den Berg, 2011; Hein, 2015). A good pore interconnectivity is observed in these facies (Fig. 7C). In HFU-II and HFU-III, the reservoir quality is affected by pore-filling cementation. The accumulation of K-feldspars, glauconite, and heavy minerals in the pore spaces blocks pore throats and reduces overall pore connectivity (Fig. 7C); these diagenetic factors are less prevalent in (HFU-I). Overall, the tidally influenced fluvial channel facies are interpreted as excellent to very good in terms of reservoir quality.

5.1.5 Tidal Flat Facies

Good-quality sandstone reservoirs, with good porosity and permeability, exist within tidal flat environments (e.g., Seaïag et al., 2016). In this study, the tidal flat facies are dominated by fine- to coarse-grained sub-feldspathic wackes (Fig. 7E), which are heterolithic at the lamination scale, and bioturbated (Fig. 5D, 4A). The grain contacts in the tidal flat facies are dominated by point contacts with few long and concavo-convex contacts, contain limited examples of intragranular microfractures, and therefore were likely exposed to low to moderate degrees of compaction. Pore-filling detrital clays are observed (Fig. 7E), which act to reduce overall reservoir quality; pore-filling residual hydrocarbons and grain-coating detrital clays (Dc) are also observed. Collectively, these observations suggest poor interconnectivity in the tidal flat facies and therefore poor reservoir quality. The heterolithic sandstone group of samples (HFU IV) has the lowest reservoir quality in the studied Abu Madi reservoir.

5.1.6 Tidal Channel Facies

Tidal channel facies can form good-quality reservoirs in petroleum systems worldwide (e.g., Weimer et al., 1982; Reinson et al., 1988). In this study, this facies are dominated by silt to fine-grained, poorly to moderately-sorted sub-feldspathic arenites and wackes (Fig. 7F). Point-to-point grain contact demonstrates that these deposits have been affected by moderate compaction (Fig. 7F). The existence of pore-filling detrital clays decreases the pore system effectiveness and reduces reservoir quality. Moderate cementation of this facies has reduced the total pore volume, with some evidence for moderate pore interconnectivity suggesting moderate reservoir quality (Fig. 7F).

To summarize, the reservoir quality of the Abu Madi reservoir is controlled by both depositional and diagenetic processes. There is an inverse relationship between the porosity and detrital clay volume, where a high detrital clay content indicates poor reservoir quality. The grain size analysis reflects some enhancement of the reservoir quality associated with the presence of coarse-grained sediments. Most sediments are poorly- to moderately-sorted. This study interprets that the abundance of detrital clays plays the main controlling parameter in reservoir quality, followed by grain size, and sorting. Reservoir quality-enhancing diagenetic controls include dissolution of cement and feldspars (Fig. 7E, B), and micro-fractures (Fig. 7E, F). On the contrary, the impacts of the reservoir quality-reducing diagenetic controls were primarily dependent on the cementation (i.e., argillaceous material and kaolinite) that led to a partial reduction of the pore network. The studied intervals displayed low to moderate degrees of compaction, and so it's influence on reservoir quality is thought to be low.

5.2. Pore systems, flow units, and links with depositional lithofacies

The Abu Madi reservoir is characterized by a wide range of facies and flow units, which reflects the variation in the depositional environment. Fluvial channel facies, tidal influenced channel facies, and the upper part of bayhead delta facies are dominated by clean sandstones, with a low clay content (average 20%). These are characterized by the highest R35 and FZI values, indicating a pore system dominated by mega-to macro-pores (FU-I and FU-II; HFU-I and HFU-II). The estuarine facies are dominated by siltstone and mudstone, as well as argillaceous sandstone, with an average clay content of 25%. The estuarine facies are characterized by moderate R35 and FZI values, indicating a pore system dominated by macro-to meso-pores (FU-III and FU-IV), and (HFU-III). Heterolithic deposits of the estuarine environment and bayhead delta sandstone facies are abundant in mudstones and argillaceous-rich sandstones. The argillaceous-rich sandstones contain an average clay content of 29%, forming poor quality reservoir intervals characterized by low R35 and FZI values, indicating a pore system dominated by micro-pores (FU-V) and (HFU-IV). The high storage and flow capacity of the Abu Madi fluvial channel facies and tidal influenced fluvial channel facies (HFU-1, HFU-2) is largely controlled by the sedimentological distribution of low detrital clay and siltstone content. In addition, reservoir quality-enhancing diagenetic controls, including dissolution of cement and feldspars (Fig. 7), and micro-fractures (Fig. 7) aid in their high reservoir performance. The storage and flow capacity of the estuarine facies/flow zones (HFU-III, HFU-IV) are low due to their high detrital clay and siltstone content. In addition, reservoir quality-reducing diagenetic controls, including cementation and compaction (Fig. 7) act to further reduce the performance of these intervals.

Despite these observations, there is no fixed relationship between the lithofacies and the petrophysical parameters (e.g., the porosity/permeability values and the HFU's/FU's), where the observed porosities and permeabilities vary across lithofacies. HFU's and FU's have been observed in both poor and excellent reservoir quality zones. This phenomenon highlights the high-degree of heterogeneity of the studied Abu Madi reservoirs, which is reported in similar studies of comparable sedimentary settings, worldwide (Moraes and Surdam, 1993; Alaa et al., 2000; Pranter et al., 2007; Luo et al., 2009; Colombera et al., 2012; Henares et al., 2016; Sahoo et al., 2016; Abdel-Fattah et al., 2022).

5.3. Implications for hydrocarbon exploration and production

The Abu Madi Formation is an important rock unit in the Nile Delta petroleum system because they contain potentially economically-significant volumes of reservoir rocks (EGPC, 1994; Dolson et al., 2005; Leila et al., 2015). As a result, investigating the petrophysical and sedimentological controls on the Abu Madi sandstone reservoir is useful for effective reservoir quality prediction, which contributes to the overall understanding of the Messinian hydrocarbon plays. A better understanding of the Abu Madi subsurface reservoirs can be gained by accurately predicting the connectivity, rock type, and flow behavior of these deposits, which ais in further reservoir simulation and modeling. The identification of five different flow units (i.e., FU-I, FU-II, FU-III, FU-IV, and FU-V) based on the application of Winland's R35 technique, as well as four HFU's (i.e., HFU-I, HFU-II, HFU-III, and HFU-IV) improves reservoir prediction and simulation for reservoir management and recovery in such heterogeneous sandstone reservoirs.

In terms of reservoir quality, the integrated core measurements, image log interpretation, and petrophysical analysis indicate that HFU-I has the highest reservoir quality, which is characterized by excellent porosity of 25–33% and excellent permeability of >900 mD. HFU-II has very good reservoir quality, which is characterized by between 17–33% porosity and very 700– 1000 mD permeability. The HFU-III has moderate to good reservoir quality, with 12–33% porosity and 4–100 mD permeability. This may shed light on the HFU-I, HFU-II, and HFU-III of the fluvial and tidally-influenced fluvial sandstones, which can now be further appraised during continued field development. HFU-IV has the lowest reservoir quality, which is characterized by low permeability (0.6–8 mD).

The inferred data from image logs allows us to define the average paleo-current direction in the studied fluvial to deltaic setting. The fluvial channel dip data shows a north-west azimuth, suggesting that the rivers were flowing in a north-westerly direction. In-comparison, the estuarine dip data shows an east to north-east dip azimuth, suggesting the marine-dominated sedimentary systems were oriented slightly oblique to the overall strike of the in-draining fluvial systems. The tidally influenced fluvial channel deposits dip data shows a north-east to north-west dip azimuth, representing the fluvial channel direction with the superimposed and opposing bi-directional marine tide direction (Fig. 10). The paleo-current direction information is important as at the field scale it can be used to guide tracking of these reservoirs across the field, and at the regional scales it provides information on the overall palaeoflow direction of the sedimentary systems during the Messinian in the Nile Delta area.

The neural log technique succeeded in predicting FZI, permeability, and petrophysical parameters in the un-cored intervals. The resulting distribution of hydraulic flow units method honored the geology of the reservoirs, as well as static and dynamic petrophysical properties. Flow units take into account both pore structure and fluid-flow performance, which improves permeability estimation and reduces the uncertainty in petrophysical assessments. Derived empirical relationships of porosity and permeability for different types of sandstone and combined empirical and theoretical models with laboratory-measured data, show a good agreement between estimated FZI and permeability and core measurements. The prediction of FZI and permeability in the non-cored intervals is of great importance in the field development and can be used in other drilled and future planned wells for production optimization.

The modified Lorenz Plot SMLP was able to improve the knowledge of the Abu Madi reservoir storage capacity and flow performance, which is controlled by five flow units in the Salma-2 well and 11 flow units in the Salma-4 well. Based on the previous results, it is concluded that the Abu Madi reservoir in the Salma-4 is more heterogeneous. In the Salma-2 well, the maximum storage and flow capacity are associated with the clean sandstones of fluvial channel deposits in the middle and lower parts of the reservoir. The low storage and flow capacity is associated with argillaceous-rich fluvial channel facies in the upper part of the reservoir. In the Salma-4 well, the main storage and flow capacity is related to tidally-influenced fluvial channel deposits and tidal channel sandstones. Flow units K and I represent low-quality reservoirs (baffles). Flow performance in the Abu Madi reservoir is primarily controlled by the character and distribution of fluvial channel and tidally influenced fluvial channel deposits, with little contribution from estuarine deposits.

Conclusions

This comprehensive integrated study has improved the geological understanding of the Messinian deposits, and in-particular the reservoir units, in the Nile Delta area. In-particular, an improved geological understanding of the Abu Madi reservoirs is provided, which exhibit multi-scalar heterogeneities in depositional environments, fluid flow, and rock types. This study demonstrates that the Abu Madi Formation in Salma Field is composed of a range of different facies, including sub-aerial gravity-flow facies, fluvial channel facies, tidal channel facies, tidal flat facies, tidally influenced fluvial channel facies, flood plain facies, and sabkha facies. The sedimentary processes responsible for depositing these facies formed a range of sandstone types, including sub-feldspathic arenites, sub-feldspathic wackes, sub-lithic arenites, feldspathic wackes, anhydrite sub-feldspathics. Reservoir quality is controlled by A combination of these depositional processes (sedimentary facies) and diagenetic processes. The abundance of detrital clays plays the main controlling parameter in reservoir quality, followed by grain size and sorting. The dissolution of cement and feldspars, along with the presence of micro-fractured grains form the main reservoir-quality-enhancing diagenetic factors, whilst pore-filling detrital clays led to a partial reduction of the pore network.

The neural log technique (K-mode) has succeeded in predicting FZI, permeability, and petrophysical parameters in the non-cored intervals. The resulting model can be used to obtain a reliable permeability prediction based on combining porosity and FZI to provide more accurate reservoir flow simulations. The Modified Lorenz Plot SMLP shows that the storage capacity and flow performance is controlled by five flow units in the Salma-2 well, whilst 11 flow units were detected in the Salma-4 well.

The Abu Madi reservoir is divided into four HFU's, including HFU-I (excellent reservoir quality and dominated by fluvial channel and tidal influenced fluvial channel facies), HFU-II (very good to good reservoir quality and dominated by fluvial channel, tidal influenced fluvial channel, and tidal channel facies, HFU-III (moderate quality sandstone dominated by tidal channel and tidal flat sandstones, with argillaceous parts of the fluvial and tidal influenced fluvial channel), and HFU-IV (low-quality reservoir and dominated by heterolithic sandstones of tidal flat facies). The storage and flow capacity of the fluvial channel facies and tidally influenced fluvial channel facies (HFU-1, HFU-2) samples are the largest due to the lower detrital clay and silt content. The storage and flow capacity of the estuarine (HFU-III, HFU-IV) facies is limited by the high detrital clay and siltstone content.

This integrated comprehensive analysis of multi-proxy datasets has yielded an improved rock type classification and petrophysical parameter distribution in heterogeneous reservoirs. The main flow in the Abu Madi reservoir is related to fluvial channel deposits and tidally influenced fluvial channel units, which better-informs the next exploration and production phases. The results of this study also contribute to the overall geological understanding of the sedimentary and stratigraphical understanding of the Messinian system in the Nile Delta area. In-particular, the relationship between interpreted sedimentary facies and depositional environment, and the spatio-stratal distribution of reservoir quality contributes greatly to the overall improved understanding of the hydrocarbon system and reservoir typology in the region.

Acknowledgment

Thanks go to the Egyptian General Petroleum Corporation (EGPC) and El-Wastani Petroleum Company for providing the required data. The authors also would like to express their depths gratitude to the guest editor, Dr. David Wood, for his great efforts in editing and enhancing the manuscript, and the reviewers for their suggestions and effective reviews. Dr. Ahmed E. Radwan is thankful to the support provided by the Priority Research Area Anthropocene under the program “Excellence Initiative—Research University” at the Jagiellonian University in Kraków.

References

Abdullah, E.A., Al-Areeq, N.M., Al-Masgari, A.A., Barakat, M. Kh., 2021a. Petrophysical evaluation of the Upper Qishn clastic reservoir in Sharyoof oil Field, Sayun-Masilah Basin, Yemen. ARPN Journal of Engineering and Applied Sciences, 2021, 16(22), pp. 2375–2394

Abdullah, E., Al-Areeq, N., Elmahdy, M., Barakat, M. Kh., 2021b. A new insight into the structural architecture of Sharyoof field, Say'un–Masilah basin, Yemen, Arabian Journal of Geosciences. 2021; 14:1977. doi.org/10.1007/s12517-021-08299-2

Abdel-Fattah, M. I., & Slatt, R. M. (2013). Sequence stratigraphic controls on reservoir characterization and architecture: case study of the Messinian Abu Madi incised-valley fill, Egypt. *Central European Journal of Geosciences*, *5*(4), 497-507.

Abdel-Fattah, M. I., Sen, S., Abuzied, S. M., Abioui, M., Radwan, A. E., & Benssaou, M. (2022). Facies analysis and petrophysical investigation of the Late Miocene Abu Madi sandstones gas reservoirs from offshore Baltim East field (Nile Delta, Egypt). Marine and Petroleum Geology, 137, 105501.

Ajdukiewicz, J. M., & Lander, R. H. (2010). Sandstone reservoir quality prediction: The state of the art. *AAPG bulletin*, *94*(8), 1083-1091.

Al-Ajmi, F.A., & Holditch, S.A., 2000. Permeability estimation using hydraulic flow units in a central Arabia reservoir, proceeding of the *SPE annual technical conference and exhibition.* SPE 63254, Dallas, Texas, October 1-4.

Alaa M. Salem,2 S. Morad,3 Luiz F. (2000). *Diagenesis and Reservoir-Quality Evolution of Fluvial Sandstones During Progressive Burial and Uplift: Evidence from the Upper Jurassic Boipeba Member, Reconcavo Basin, Northeastern Brazil. AAPG Bulletin, 84.* doi:10.1306/a9673b9e-1738-11d7-8645000102c1865d

Al-Farisi, O., Elhami, M., Al-Felasi, A., Yammahi, F., Ghedan, S., 2009. Revelation of carbonate rock typing - the resolved gap. *Paper SPE 125576, SPE/EAGE Res.* Charact. Simul. Conf. 19-21 Oct., Abu Dhabi, UAE.

Al-Ibadi, H., Al-Jawad, S.N., 2020. Permeability Evaluation of Carbonate Reservoir Using Hydraulic Unit Analyse: Case Study from Middle East Region, *82nd EAGE Conference & Exhibition* Amsterdam, The Netherlands.

Allen, J. R. L. (1982). Mud drapes in sand-wave deposits: a physical model with application to the Folkestone Beds (early Cretaceous, southeast England). *Philosophical Transactions* *of the Royal Society of London. Series A, Mathematical and Physical Sciences*, *306*(1493), 291-345.

Ali, A.M., Radwan, A.E., Abd El-Gawad, E.A., Abdel-Latief, A. A., 2021. 3D Integrated Structural, Facies and Petrophysical Static Modeling Approach for Complex Sandstone Reservoirs: A Case Study from the Coniacian–Santonian Matulla Formation, July Oilfield, Gulf of Suez, Egypt. Nat Resour Res. https://doi.org/10.1007/s11053-021-09980-9

Amaefule, J., Altunbay, M., Tiab, D., Kersey, D., Keelan, D., 1993. Enhanced reservoir description, using core and log data to identify hydraulic (flow) units and predict permeability in uncored intervals/wells: SPE 26436, *annual technical conference and exhibition*, Houston, TX, pp 3–6.

Archie, G., 1942. The electric resistivity logs as an aid in determining some reservoir characteristics. *Trans Am Int Mech Eng*, 146, 54-62.

Barakat, M. Kh., 2010. Modern geophysical techniques for constructing a 3D geological model on the Nile Delta, Egypt. *PhD Dissertation: Technische Universität Berlin*, 158.

Barakat, M. Kh., Dominik, W., 2010. Seismic studies on the Messinian rocks in the onshore Nile Delta, Egypt, *72nd EAGE Conference, and Exhibition*: 7, pp. 5422–5426.

Barakat, M. Kh., Nooh, A. Z., 2017. Reservoir quality using the routine core analysis data of Abu Roash "C" in Badr El Din-15 oil field, Abu Gharadig basin, north Western Desert, Egypt. *Journal of African Earth Sciences*, 129, 683-691.

Barakat, M., El-Gendy, N., El-Bastawesy, M., 2019. Structural modeling of the Alam El-Bueib Formation in the jade oil field, Western Desert, Egypt J. Afr Earth Sci 156:168–177

Barakat, M. Kh., El-Gendy, N., El-Nikhely, A., Zakaria, A., Hellish, H., 2021. Challenges of the Seismic Image Resolution for Gas Exploration in the East Mediterranean Sea. Journal of Petroleum and Mining Engineering 23(2)2021. DOI: 10.21608/jpme.2021.86935.1092.

Barakat, M. Kh, Azab, A. A, Nabil, M. 2022. Reservoir Characterization Using the Seismic Reflection Data: Bahariya Formation as a Case Study Shushan Basin, North Western Desert, Egypt. Journal of Petroleum and Mining Engineering. 2022; 24(1) p.1-11, 2021.DOI: 10.21608/jpme.2022.110315.1107

Barber, P., 1981. Messinian subaerial erosion of the proto-Nile Delta, *Mar Geol* 44:253–272.

Bear, J.,1972. Dynamics of fluids in porous media. *American Elsevier Publishing Company*, New York, p 764.

Beiranvand, B., Kamali, M. R., 2004. Petrophysical evaluation and determination of rock types in a carbonate reservoir in SW Iran with interpretation of petrography and geophysical well logs. *Iranian International Journal of Science*, 5(2), 203– 221.

Bernabé, Y., Mok, U., Evans, B., 2003. Permeability-porosity relationships in rocks subjected to various evolution processes. *Pure and Applied Geophysics*; 160(5): 937-60.

Bhatt, A., Helle, H.B., Ursin, B., 2001. Application of committee machines in reservoir Characterization while drilling: "a novel neural network approach in log analysis" *Brisbane, Australia, 16–18 October*.

Bhattacharya, J.P., 1992. Deltas, In: Facies Models (Ed. byR. G. Walker &N. P. James), pp. 157^ 177. Geological Association of. Citeseer.

Blair, T.C., & McPherson, J.G., (1994). Alluvial fans and their natural distinction from rivers based on morphology, hydraulic processes, sedimentary processes, and facies: *Journal of Sedimentary Research*, v. A64, p. 451–490.

Bridge, J., 2006. Fluvial facies models, recent Developments Posamentier, H.; Walker, R. (Eds.): Facies Models Revisited. *SEPM 84. Spec. Publ.,* pp. 85–170.

Buatois, L., Mángano, M., Carr, T., 1999. Sedimentology and ichnology of Paleozoic estuarine and shoreface reservoirs, Morrow sandstone, lower Pennsylvanian of southwest Kansas, USA. *Kansas Geological Survey Bulletin 243*. Current Research Earth Science.

Carmen, P.C., 1937. Fluid Flow through Granular Beds. Trans. *AIChE 15*, 150-166.

Chopra, A.K., Stein, M.H. Ader, J.C., 1998. Development of reservoir descriptions to aid in the design of EOR projects. *SPE reservoir engineering*, 16370.

Colombera, L., Felletti, F., Mountney, N. P., & McCaffrey, W. D. (2012). A database approach for constraining stochastic simulations of the sedimentary heterogeneity of fluvial reservoirs. *AAPG bulletin*, *96*(11), 2143-2166.

Corbett, P. W., & Jensen, J. L. (1992). Variation of reservoir statistics according to sample spacing and measurement type for some intervals in the Lower Brent Group. *The Log Analyst*, *33*(01).

Corbett, P. W. M., & Duarte, G. L. B. (2019). Understanding subsurface fluvial architecture from a combination of geological well test models and well test data. *Geological Society, London, Special Publications*, *488*(1), 237-257.

Corbett, P. (2009). *Petroleum Geoengineering: integration of static and dynamic models*. Society of Exploration Geophysicists and European Association of Geoscientists and Engineers.

Costa, A., 2006. Permeability-porosity relationship: a reexamination of the Kozeny-Carman equation based on a fractal pore-space geometry assumption. *Geophysical research letters;* 33(2): L02318.

Dalla, S., Hamed, H., Serrazi, M., 1997. Hydrocarbon exploration in a complex incised valley fill, An example from the late Messinian Abu Madi Formation (Nile Delta basin, Egypt). *Leading-edge*, pp 1819–1824.

Demyanov, V., Backhous, L., Christi, M., 2015. Geological feature selection in reservoir modeling and history matching with Multiple Kernel Learning. *Computers & Geosciences*, 85, 16–25.

Dolson, C. J., Shaan, V. M., Matbouly, S., Harwood, C., Rashed, R., Hammouda, H., 2001. The petroleum potential of Egypt. – In Downey, W.M.; Threet, C. J., and Morgan, A. W. (Eds.): Petroleum provinces of the twenty-first century., Memoir No. 74, 453-482, *American Association of Petroleum Geologists*, Tulsa, Oklahoma.

Dolson, J.C., Boucher P.J., Siok J., Heppard, P., 2005. Key challenges to realizing the full potential in an emerging giant gas province, Nile Delta/Mediterranean offshore, deep water, Egypt. In: Doré A, Vining B (eds)Petroleum geology, north-west Europe and global perspectives, Geological Society of London, petroleum geology conference series no. 6, *proceedings of 6th petroleum geology conference*, pp 607–624.

Donselaar, M. E., & Schmidt, J. M. (2005). Integration of outcrop and borehole image logs for high-resolution facies interpretation: example from a fluvial fan in the Ebro Basin, Spain. *Sedimentology*, *52*(5), 1021-1042.

Dott, R.H., 1964. Wacke, greywacke, and matrix: what approach to immature sandstone classification? *Journal of Sedimentary Petrology*, 34, pp.623-632.

Dubois, M.K., Byrnes, A.P., Bhattacharya, S., Bohling, G.C., Doveton, J.H., Barba, R.E., 2006. Hugoton asset management Project (HAMP). *Hugoton geo model final report*. KGS open file report.

EGPC (Egyptian General Petroleum Corporation) 1994. Nile Delta and North Sinai, field discoveries and hydrocarbon potentials (A comprehensive overview). *EGPC,* Cairo, p 387.

El-Adl, H., Leila, M., Ahmed, A., Anan, T., El-Shahat, A., 2021. Integrated sedimentological and petrophysical rock-typing of the Messinian Abu Madi Formation in South Batra gas field, onshore Nile Delta, Egypt. *Marine and Petroleum Geology* 124 (2021) 104835.

El-Gendy, N., Barakat, M., Abdallah, H., 2017. Reservoir assessment of the Nubian sandstone reservoir in South Central Gulf of Suez Egypt. *Journal of African Earth Sciences,* 129, 596–609.

El-Gendy, N., Abuamarah, B.A., Nabawy, B.S., Ghrefat, H., Kassem, O., 2020. Pore fabric anisotropy of the Cambrian–Ordovician Nubia sandstone in the Onshore Gulf of Suez, Egypt: a surface outcrop analog. *Nat Resour Res* 29(2):1307–1328.

Elias, A. R., De Ros, L. F., Mizusaki, A. M., & Anjos, S. M. (2004). Diagenetic patterns in eolian/coastal sabkha reservoirs of the Solimões Basin, northern Brazil. *Sedimentary Geology*, *169*(3-4), 191-217.

El-Nikhely, A., El-Gendy, N. H., Bakr, A. M., Zawra, M. S., Ondrak, R., & Barakat, M. K. (2022). Decoding of seismic data for complex stratigraphic traps revealing by seismic attributes analogy in Yidma/Alamein concession area Western Desert, Egypt. *Journal of Petroleum Exploration and Production Technology*, 1-14. https://doi.org/10.1007/s13202-022-01527-9

El-Sharawy, M. S., Nabawy, B. S., 2019. Integration of electrofacies and hydraulic flow units to delineate reservoir quality in uncored reservoirs: A case study, Nubia Sandstone Reservoir, Gulf of Suez, Egypt. *Natural Resources Research*, 28.

El-Sharawya, M., Leila, M., Bakr, A., Kamela, A., 2020. Petrophysical evaluation of the Messinian Abu Madi Formation in Salma delta gas field, northeastern onshore Nile Delta, Egypt. *Journal of Environmental Sciences*, 2020; Vol. 49, No. 2: 46-53.

Ezekwe, J. N., Filler, S. L., 2005. Modeling Deepwater Reservoirs. paper *SPE 95066 presented at the SPE Annual Technical Conference and Exhibition held in Dallas*, Texas, USA.

Folkestad, A., Veselovsky, Z., & Roberts, P. (2012). Utilising borehole image logs to interpret delta to estuarine system: A case study of the subsurface Lower Jurassic Cook Formation in the Norwegian northern North Sea. *Marine and Petroleum Geology*, *29*(1), 255-275.

Gandhi, A., Torres-Verdín, C., Voss, B., Gabulle, J., Seminario, F., 2010. Construction of Reliable Static and Dynamic Multi-Layer Petrophysical Models in Camisea Gas Reservoirs, Peru. *SPWLA 51st Annual Logging Symposium*, Perth, Australia.

Gargani, J., Rigollet, C., Scarselli, S., 2010. Isostatic response and geomorphological evolution of the Nile valley during the Messinian salinity crisis. *Bull. Soc. Geol*. Fr. 181, 19–26.

Chandra, V., Barnett, A., Corbett, P., Geiger, S., Wright, P., Steele, R., & Milroy, P. (2015). Effective integration of reservoir rock-typing and simulation using near-wellbore upscaling. *Marine and Petroleum Geology*, *67*, 307-326.

Gibling, MR. 2006. Width and thickness of fluvial channel bodies and valley fills in the geological record: a literature compilation and classification. J Sediment Res.;76(5):731–70. https://doi.org/10.2110/jsr.2006.060.

Gomes, J.S., Riberio, M.T., Strohmenger, C.J., Negahban, S., Kalam, M.Z., 2008. Carbonate reservoir rock typing the link between geology and SCAL. *SPE paper 118284.*

Gunter, G., Finneran, H., Hartmann, D., Miller, J., 1997. Early determination of reservoir flow units using an integrated petrophysical method. In: *SPE Ann. Tech, Conf., and Exhib.,* SPE Paper 38679, pp. 8.

Guo, G., Diaz, M.A., Paz F., Smalley, J., Waninger, E.A. 2005. Rock typing is an effective tool for permeability and water saturation modeling, a case study in a clastic reservoir in the Oriente basin. Paper SPE 97033, presented at the OSPE. *Annual technical conference and exhibition,* Dallas, Texas, USA.

Hassan, S., Darwish, M., Tahoun, S. S., & Radwan, A. E. (2022). An integrated high-resolution image log, sequence stratigraphy and palynofacies analysis to reconstruct the Albian–Cenomanian basin depositional setting and cyclicity: Insights from the southern Tethys. *Marine and Petroleum Geology*, *137*, 105502.

Heidari Z., Torres-Verdín C., Preeg, W. E., 2012. Improved estimation of mineral and fluid volumetric concentrations in thinly bedded and invaded Formations. *Geophysics*, 77 (3): WA79 – WA98.

Heidari, Z., Torres-Verdín, C., Mendoza, A., Wang, G.L., 2011. Assessment of Residual Hydrocarbon Saturation with the Combined Quantitative Interpretation of Resistivity and Nuclear Logs. *Petrophysics*, 52 (3): 217 - 237.

Hein, F. J. (2015). The Cretaceous McMurray oil sands, Alberta, Canada: A world-class, tidally influenced fluvial–estuarine system—an Alberta government perspective. In *Developments in Sedimentology* (Vol. 68, pp. 561-621). Elsevier.

Henares, S., Caracciolo, L., Viseras, C., Fernández, J., & Yeste, L. M. (2016). Diagenetic constraints on heterogeneous reservoir quality assessment: A Triassic outcrop analog of meandering fluvial reservoirs. *AAPG Bulletin*, *100*(9), 1377-1398.

Hunger, O., Evans, S., Bovis, M., Hutchinson, J., 2001. A review of the classification of landslides of the flow type. *Env. Eng. Geosci* vii (3), 221–238.

Jensen, J., Lake, L. W., Corbett, P. W., & Goggin, D. (2000). *Statistics for petroleum engineers and geoscientists* (Vol. 2). Gulf Professional Publishing.

Jones, R. R., McCaffrey, K. J. W., Clegg, P., Wilson, R. W., Holliman, N. S., Holdworth, R. E., 2009. Integration of regional to outcrop digital data: 3D visualization of multiscale geological models. *Computers & Geosciences*, 35(1), 4– 18.

Katz, A.J., Thompson, A.H., 1986. Quantitative Prediction of Permeability in Porous Rock, *Physical Review* B, 34, 8179-8181.

Kinsman, D.J., 1969. Mode of Formation, sedimentary association, and diagnostic features of shallow water and supratidal evaporites. *Am. Assoc. Pet. Geol. Bull*., 53: 830-840.

Klein, G., 1971. A sedimentary model for determining paleotidal range. *Geol. Soc. Am. Bull*. 82, 2585–2592.

Kolodzie, S., 1980. Analysis of pore throat size and use of the Waxmann–Smits equation to determine OOIP in Spindle Field, Colorado. In: Proceedings society of petroleum engineers, *55th annual technical fall conference SPE-9382*.

Kozeny, J., 1927. Uber kapillare letung des wassers im boden, Sitzungsberichte, *Royal Academy of Science, Vienna, Proc. Class I*, 136, 271-306.

Lagraba, P., Javier, O., Hansen, S.M., Spalburg, M., Helmy, M., (2010). Borehole Image Tool Design, Value of InFormation, and Tool Selection, PÖppelreiter, M., Garcı´a-Carballido, C., and Kraaijveld, M., eds., Dipmeter and borehole image log technology: AAPG Memoir 92, 15–38.

Lai, J., Wang, G., Wang, S., et al. (2018). A review on the applications of image logs in structural analysis and sedimentary characterization. Marine and Petroleum Geology, 95, 139-166.

Leila, M., El Sharawy, M., Mohamed, A., Gorini, C., Bucci, M. G., Radwan, A. E., & Moretti, M. 2022a. Soft-sediment deformation structures in the Late Messinian Abu Madi Formation, onshore Nile Delta, Egypt: Triggers and tectonostratigraphic implications. *Geological Journal*.

Leila, M., El Sharawy, M., Bakr, A., & Mohamed, A. K. 2022b. Controls of facies distribution on reservoir quality in the Messinian incised-valley fill Abu Madi Formation in Salma delta gas field, northeastern onshore Nile Delta, Egypt. *Journal of Natural Gas Science and Engineering*, *97*, 104360.

Leila, M., Moscariello, A., 2019. Seismic stratigraphy and sedimentary facies analysis of the pre-and syn-Messinian salinity crisis sequences, onshore Nile Delta, Egypt. Implications for reservoir quality prediction. *Mar Petrol Geol* 101:303–321.

Leila, M., Ali, E., Abu El-Magd, A., AlWaan, L., Elgendy, A., 2020b. Formation evaluation and reservoir characteristics of the Messinian Abu Madi sandstones in Faraskour Gas Field, onshore Nile Delta, Egypt. *J. Petrol. Expl. Prod. Tech.,* https://doi.org/10.1007/s13202-020-01011-2.

Leila, M., Kora, M., Ahmed, M., Ghanem, A., 2015. Sedimentology and reservoir characterization of the upper Miocene, Qawasim Formation, El-Tamad oil field onshore, Nile Delta, Egypt. *Arab J Geosci* 9:1–13.

Leverett, M.C., 1941. Capillary behavior in porous solids. *Transactions of the AIME*, 142 (1): 159 - 172.

Lucia, F.J., 2007. Carbonate reservoir characterization. *Springer-Verlag Berlin Heidelberg,* 341p.

Luo, J. L., Morad, S., Salem, A., Ketzer, J. M., Lei, X. L., Guo, D. Y., & Hlal, O. (2009). Impact of diagenesis on reservoir-quality evolution in fluvial and lacustrine-deltaic sandstones: evidence from Jurassic and Triassic sandstones from the Ordos Basin, China. *Journal of Petroleum Geology*, *32*(1), 79-102. doi:10.1111/j.1747-5457.2009.004

Mac Eachern, J. Bann, K. 2008. The role of ichnology in refining shallow marine facies models: recent advances in models of siliciclastic shallow marine stratigraphy. In: In Hampson, J., Steel, R., Burgess, P., Dalrymple, R. (Eds.), *SEPM Spec. Publ,* vol. 90. pp. 73–116.

Masalmeh, S.K., Wei, L., Hillgartner, H., Al-Mjeni, Blom, C.R., 2012. Developing high resolution 907 static and dynamic models for water-flood history matching and EOR evaluation of a 908 Middle Eastern carbonate reservoir. *Paper SPE 161485*, Int. Petrol. Conf. 909 Ex., Abu Dhabi, UAE.

Maschio, C., Vidal, A. C., Schiozer, D. J., 2008. A framework to integrate history matching and geostatistical modeling using genetic algorithm and direct search methods. *Journal of Petroleum Science and Engineering,* 63(1), 34–42.

Martinius, A. W., & Van den Berg, J. H. (2011). *Atlas of sedimentary structures in estuarine and tidally-influenced river deposits of the Rhine-Meuse-Scheldt system* (p. 298). Houten: EAGE.

Miall, A. D. (1988). Reservoir heterogeneities in fluvial sandstones: lessons from outcrop studies. *AAPG bulletin*, *72*(6), 682-697.

Miall, A., 1977. A review of the braided river depositional environment. *Earth Sci. Rev.,* 13, 1-62.

Miall, A. D. (2014). *Fluvial depositional systems* (Vol. 14, p. 316). Cham: Springer International Publishing.

Mirzaei-Paiaman, A., Ostadhassan, M., Rezaee, R., Saboorian, H., Chen, Z., 2018. A new approach in petrophysical rock typing. *Journal of Petroleum Science and Engineering,* 166, 445–464.

Morad, S., Al-Ramadan, K., Ketzer, J. M., & De Ros, L. F. (2010). The impact of diagenesis on the heterogeneity of sandstone reservoirs: A review of the role of depositional facies and sequence stratigraphy. *AAPG bulletin*, *94*(8), 1267-1309.

Moraes, M. A., & Surdam, R. C. (1993). Diagenetic heterogeneity and reservoir quality: Fluvial, deltaic, and turbiditic sandstone reservoirs, Potiguar and Reconcavo rift basins, Brazil. *AAPG Bulletin*, *77*(7), 1142-1158.

Nabawy, B. S., Barakat, M. Kh., 2017. Formation evaluation using conventional and special core analyses: Belayim Formation as a case study, Gulf of Suez, Egypt. *Arabian Journal of Geosciences,* 10(25), 1–23.

Nabawy, B. S., Basal, A. M. K., Sarhan, M. A., Safa, M. G., 2018a. Reservoir zonation, rock typing and compartmentalization of the Tortonian-Serravallian sequence, Temsah Gas Field, offshore Nile Delta, Egypt. *Marine and Petroleum Geology* ,92 ,609–631.

Nabawy, B. S., Rashed, M. A., Mansour, A. S., Afify, W. S. 2018b. Petrophysical and microfacies analysis as a tool for reservoir rock typing and modeling: Rudeis Formation, off-shore October Oil Field, Sinai. *Marine and Petroleum Geology*, 97, 260–276.

Nabawy, B.S., El-Gendy, N. Gazia, M., 2020. Mineralogic and diagenetic controls on reservoir quality of Paleozoic sandstones, Gebel El-Zeit, North Eastern Desert, Egypt*. Nat Resour Res* 29(2):1215–1238.

Nabawy, B.S., Lashin, A., Barakat, M. Kh., 2022a. Implementation of lithofacies and microfacies types on reservoir quality and heterogeneity of the Late Cretaceous Upper Bahariya Member in the Shurouk Field, Shoushan Basin, North Western Desert, Egypt. Journal of Asian Earth Sciences DOI: 10.1016/j.jseaes.2022, 224, 105014.

Nabawy, B. S., Abudeif, A. M., Masoud, M. M., & Radwan, A. E. 2022b. An integrated workflow for petrophysical characterization, microfacies analysis, and diagenetic attributes of the Lower Jurassic type section in northeastern Africa margin: Implications for subsurface gas prospection. *Marine and Petroleum Geology*, 105678.

Novak, K., Malvik, T., Velic J., Simon, K., 2014. Increased hydrocarbon recovery and CO2 storage in Neogene sandstones, a Croatian example: *part II. Environ Earth Sci* 71(8):3641–3653.

Palmieri, G., Harby, H., Martini, J., Hashem, F., Dalla, S., Shash, M., 1996. Baltim fields complex, an outstanding example of hydrocarbon accumulations in a fluvial Messinian incised valley. In: *Proceedings of 13th EGPC exploration and production conference* Cairo, Egypt, vol 1, pp 256–269.

Panda, M.N., Lake, L.W., 1994. Estimation of single-phase permeability from parameters of particle-size distribution. *American association of petroleum geologists bulletin*, 78(7):1028e39.

Pittman, E., 1992. Relationship of porosity and permeability to various parameters derived from mercury injection-capillary pressure curves for sandstone*. AAPG Bull* 76:191–198.

Poupon, A., Leveaux, J., 1971. Evaluation of Water Saturation in Shaly Formations. *SPWLA 12th Annual Logging Symposium, Society of Petrophysicists and Well-Log Analysts.*

Pranter, M. J., Ellison, A. I., Cole, R. D., & Patterson, P. E. (2007). Analysis and modeling of intermediate-scale reservoir heterogeneity based on a fluvial point-bar outcrop analog, Williams Fork Formation, Piceance Basin, Colorado. AAPG bulletin, 91(7), 1025-1051.

Radwan, A. E., 2022b. Chapter Two - Three-dimensional gas property geological modeling and simulation. Chapter 2 in, Wood, D.A., Cai, J. (Eds.) Sustainable geoscience for natural gas sub-surface systems, Elsevier. p. 29-45. [*https://doi.org/10.1016/B978-0-323-85465-8.00011-X*](https://doi.org/10.1016/B978-0-323-85465-8.00011-X)

Radwan, A. E. 2022a. Provenance, depositional facies, and diagenesis controls on reservoir characteristics of the middle Miocene Tidal sandstones, Gulf of Suez Rift Basin: Integration of petrographic analysis and gamma-ray log patterns*. Environmental Earth Sciences, 81(15), 1-15.*

Radwan, A.E., 2021. Modeling the Depositional Environment of the Sandstone Reservoir in the Middle Miocene Sidri Member, Badri Field, Gulf of Suez Basin, Egypt: Integration of Gamma-Ray Log Patterns and Petrographic Characteristics of Lithology. Nat Resour Res 30, 431–449*. https://doi.org/10.1007/s11053-020-09757-6*

Radwan, A. E., Abudeif, A. M., & Attia, M. M. 2020. Investigative petrophysical fingerprint technique using conventional and synthetic logs in siliciclastic reservoirs: A case study, Gulf of Suez basin, Egypt. Journal of African Earth Sciences, 167, 103868. https://doi.org/10.1016/j.jafrearsci.2020.103868

Radwan, A. E., Wood, D. A., Abudeif, A. M., Attia, M.M., Mahmoud, M., Kassem A.A., Kania, M., 2021c. Reservoir Formation Damage; Reasons and Mitigation: A Case Study of the Cambrian–Ordovician Nubian 'C' Sandstone Oil and Gas Reservoir from the Gulf of Suez Rift Basin. Arabian Journal for Science and Engineering. *https://doi.org/10.1007/s13369-021-06005-8*

Radwan, A.E., Nabawy, B.S., Kassem, A.A., Hussein, W., 2021b. Implementation of Rock Typing on Waterflooding Process During Secondary Recovery in Oil Reservoirs: A Case Study, El Morgan Oil Field, Gulf of Suez, Egypt. Nat Resour Res. *https://doi.org/10.1007/s11053-020-09806-0*

Radwan, A. E., Rohais, S., Chiarella, D., 2021a. Combined stratigraphic-structural play characterization in hydrocarbon exploration: a case study of Middle Miocene sandstones, Gulf of Suez basin, Egypt. Journal of Asian Earth Sciences, 104686. *https://doi:10.1016/j.jseaes.2021.104686*

Reinson, G. E., Clark, J. E., & Foscolos, A. E. (1988). Reservoir geology of Crystal Viking field, Lower Cretaceous estaurine tidal channel-bay complex, south-central Alberta. *AAPG bulletin*, *72*(10), 1270-1294.

Ringrose, P., & Bentley, M. (2016). *Reservoir model design*. Berlin, Germany: Springer.

Sahoo, H., Gani, M. R., Hampson, G. J., Gani, N. D., & Ranson, A. (2016). Facies-to sandbody-scale heterogeneity in a tight-gas fluvial reservoir analog: Blackhawk Formation, Wasatch Plateau, Utah, USA. *Marine and Petroleum Geology*, *78*, 48-69.

Salazar, J. M., Torres-Verdín, C., Alpak, F. O., Habashy, T. M., Klein, J. D., 2006. Estimation of permeability from array induction measurements: applications to the petrophysical assessment of tight-gas sands. *Petrophysics*, 47 (6): 527 - 544.

Salem, A. M., Ketzer, J. M., Morad, S., Rizk, R.R., Al-Aasm, I. S. 2005. Diagenesis and reservoir quality evolution of incised valley sandstones, evidence from the Abu Mad gas reservoirs (Upper Miocene), the Nile Delta Basin, *Egypt. J. Sed. Res.*, 75, 572- 584.

Saïag, J., Brigaud, B., Portier, É., Desaubliaux, G., Bucherie, A., Miska, S., & Pagel, M. (2016). Sedimentological control on the diagenesis and reservoir quality of tidal sandstones of the Upper Cape Hay Formation (Permian, Bonaparte Basin, Australia). *Marine and Petroleum Geology*, *77*, 597-624.

Selim, S. S. (2018). Sedimentological architecture, shelf-edge trajectories and evolution of an Oligocene reservoir, East Nile Delta. *Geological Magazine*, *155*(3), 747-771.

Skalinski, M., Kenter, J.M., 2014. Carbonate petrophysical rock typing: integrating geological attributes and petrophysical properties while linking with dynamic behavior. In: Agar, S.M., Geiger, S., (eds.), Fundamental Controls on Fluid Flow in Carbonates. *Geol. Soc. London, Spec*. Publ., 406, 229-259.

Soleimani, M., Shokri, B. J., 2015. 3D static reservoir modeling by geostatistical techniques used for reservoir characterization and data integration. *Environmental Earth Science*, 74, 1403–1414.

Soleimani, M., Shokri, B.J., Rafiei, M. 2017. Integrated petrophysical modeling for a strongly heterogeneous and fractured reservoir, Sarvak Formation, SW Iran. *Natural Resources Research,* 26(1), 75-88.

Taylor, T. R., Giles, M. R., Hathon, L. A., Diggs, T. N., Braunsdorf, N. R., Birbiglia, G. V., Espejo, I. S. (2010). Sandstone diagenesis and reservoir quality prediction: Models, myths, and reality. *AAPG bulletin*, *94*(8), 1093-1132.

Terwindt, J., 1971. Litho-facies of inshore estuarine and tidal-inlet deposits. *Geol Mijnbouw*, 50(3):515–526.

Tiab, D., Donaldson, E.C. 1996. Petrophysics; Theory and Practice of Measuring Reservoir Rock and Fluid Transport Properties. Houston, TX: Gulf Publishing.926p.

Tucker, M., 1988. Techniques in Sedimentology. *Blackwell Scientific Publications*, 394p.

Tucker, M., 2001. Sedimentary Petrology. *Blackwell Scientific, Oxford*, pp. 272.

Van den Berg, J., Boersma, J., Van Gelder, A., 2007. Diagnostic sedimentary structures of the fluvial-tidal transition zone- evidence from deposits of the Rhine and Meuse. *Neth J Geosci,* 86:306–387.

Varavur, S., Shebl, H., Salman, S.M., Shibasaki, T., Dabbouk, C. 2005. Reservoir rock type definition in a giant cretaceous carbonate. *Society of petroleum engineers,* paper no. 93477.

Weimer, R. J., Howard, J. D., Lindsay, D. R., Scholle, P. A., & Spearing, D. (1982). Tidal flats and associated tidal channels. In *Sandstone depositional environments* (Vol. 31, pp. 191-245). American Association of Petroleum Geologists Tulsa, Okla.

Worden, R. H., & Burley, S. D. (2003). Sandstone diagenesis: the evolution of sand to stone. *Sandstone diagenesis: Recent and ancient*, *4*, 3-44.

Yehia, I., Elbarkooky, A. A., Wazery, M., Saad, T., 2019. Integrated regional study for Messinian, onshore eastern Nile Delta, Egypt.” *Mediterranean Offshore Conferences,* Egypt.

<u>List of Figures</u>

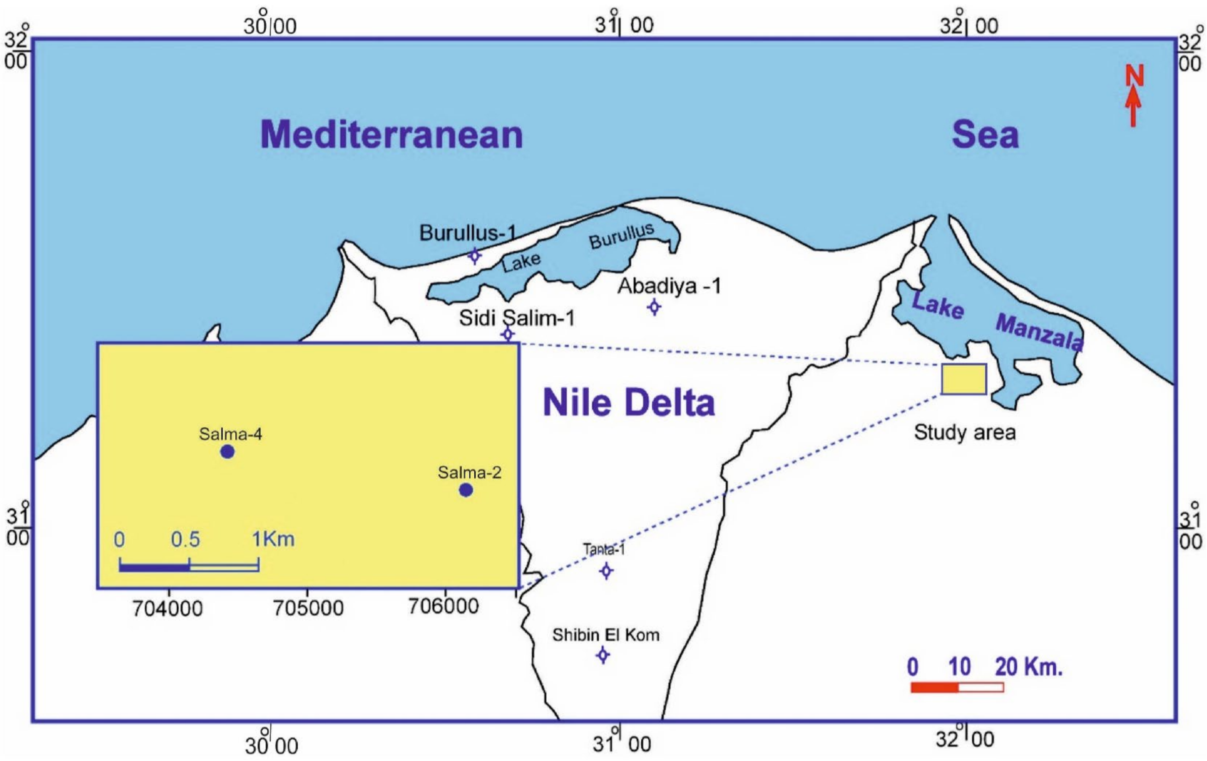

Fig.1: Location map of Salma Field.

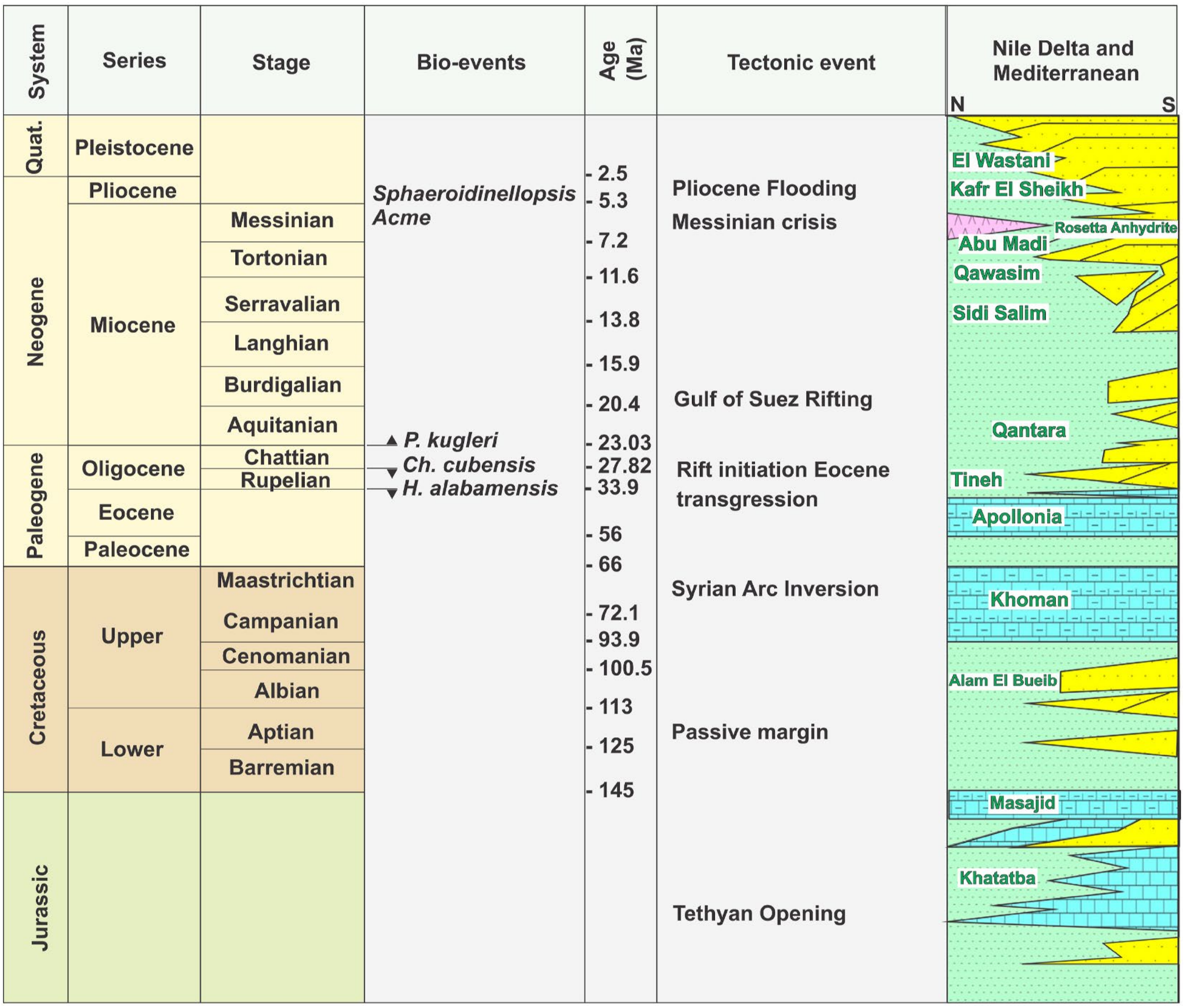

Fig.2: Tectonostratigraphic framework of the Nile Delta and Mediterranean (modified after Dolson et al., 2014). Ch. cubensis = Chiloguembelina cubensis; H. alabamensis =Hantkenina alabamensis; P. Kugleri = Paragloboratalia Kugleri; Quat. = Quaternary.

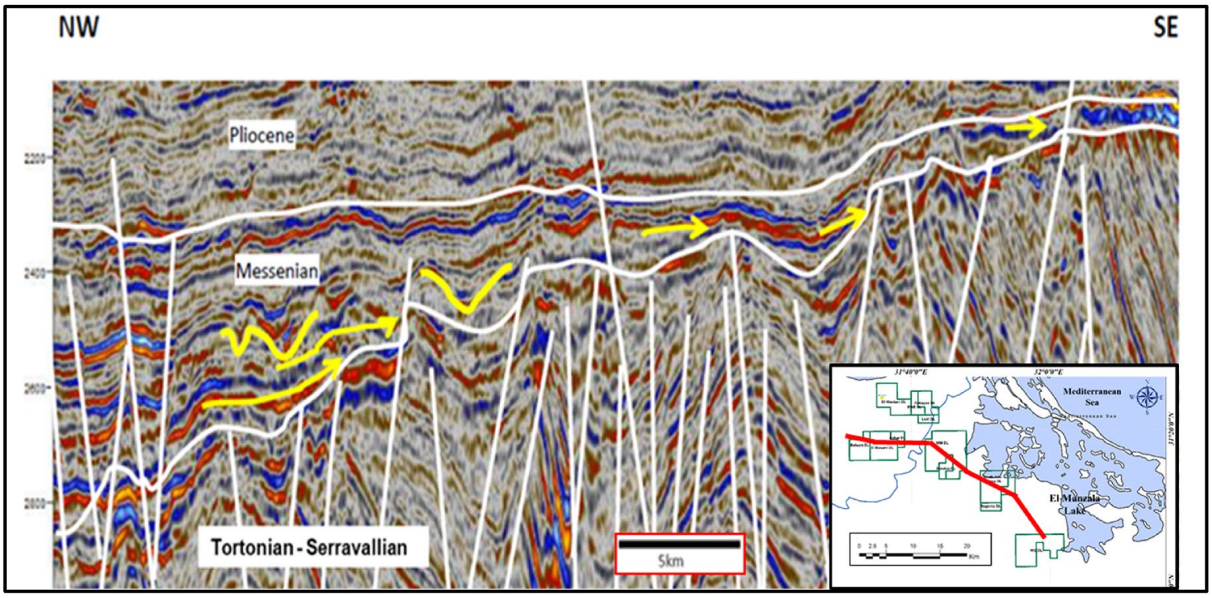

Fig. 3: Regional east Nile Delta Messenian depositional trends (Yehia et al., 2019).

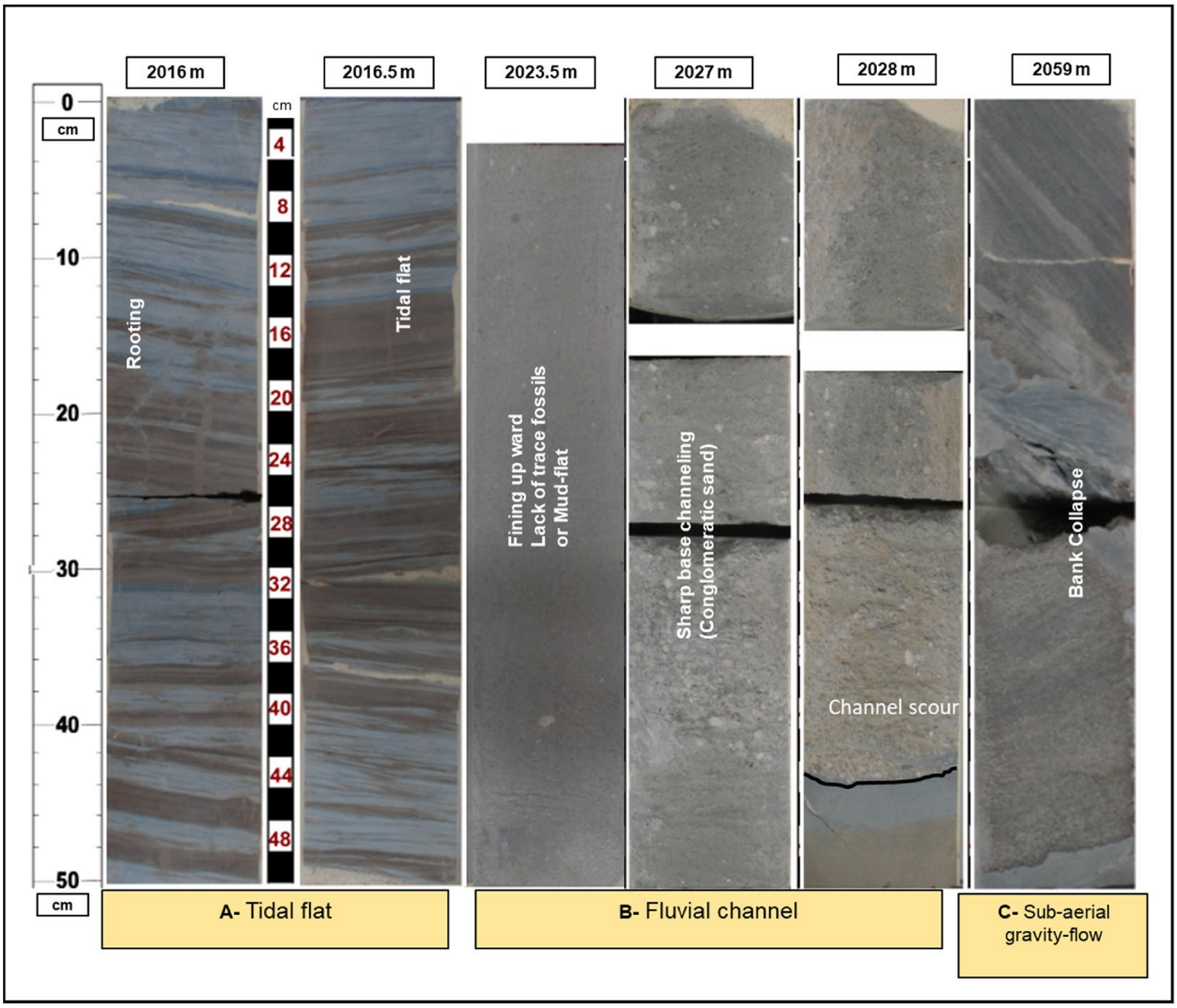

Fig. 4: Core photos showing the sedimentary facies of Abu Madi Formation in Salma-2 well.

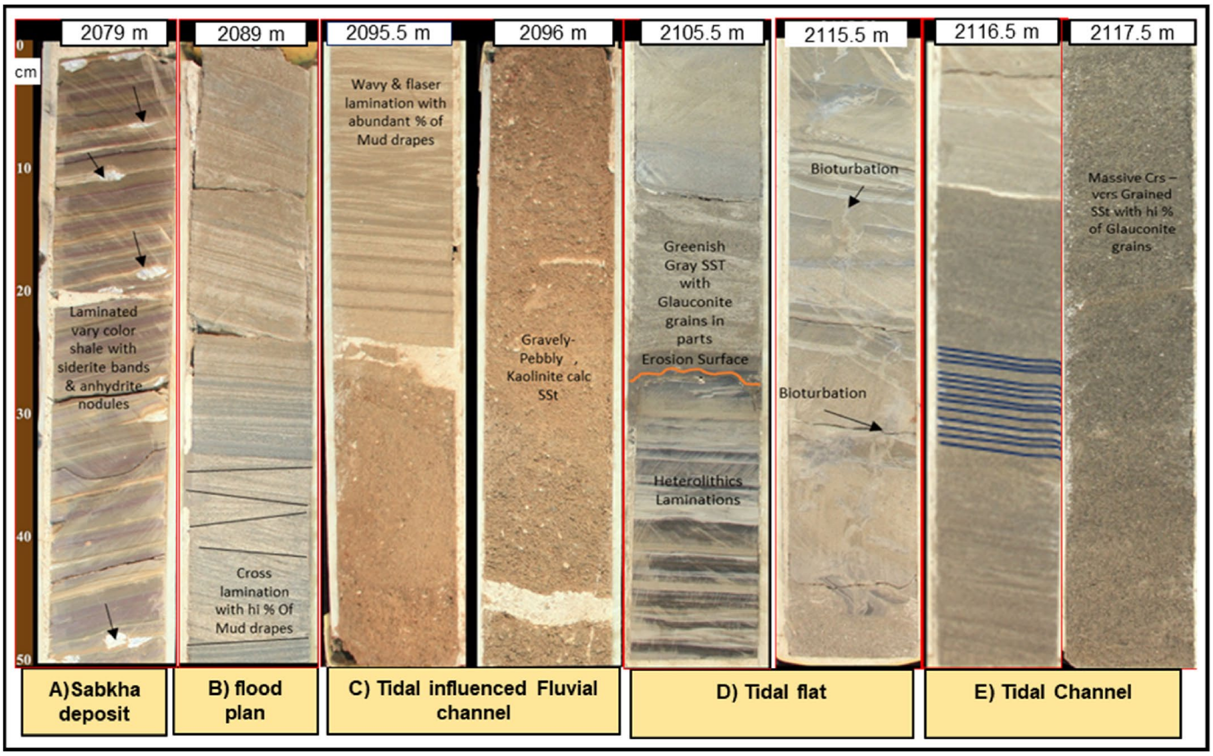

Fig. 5: Core photos showing the sedimentary facies of Abu Madi Formation in Salma-4 well.

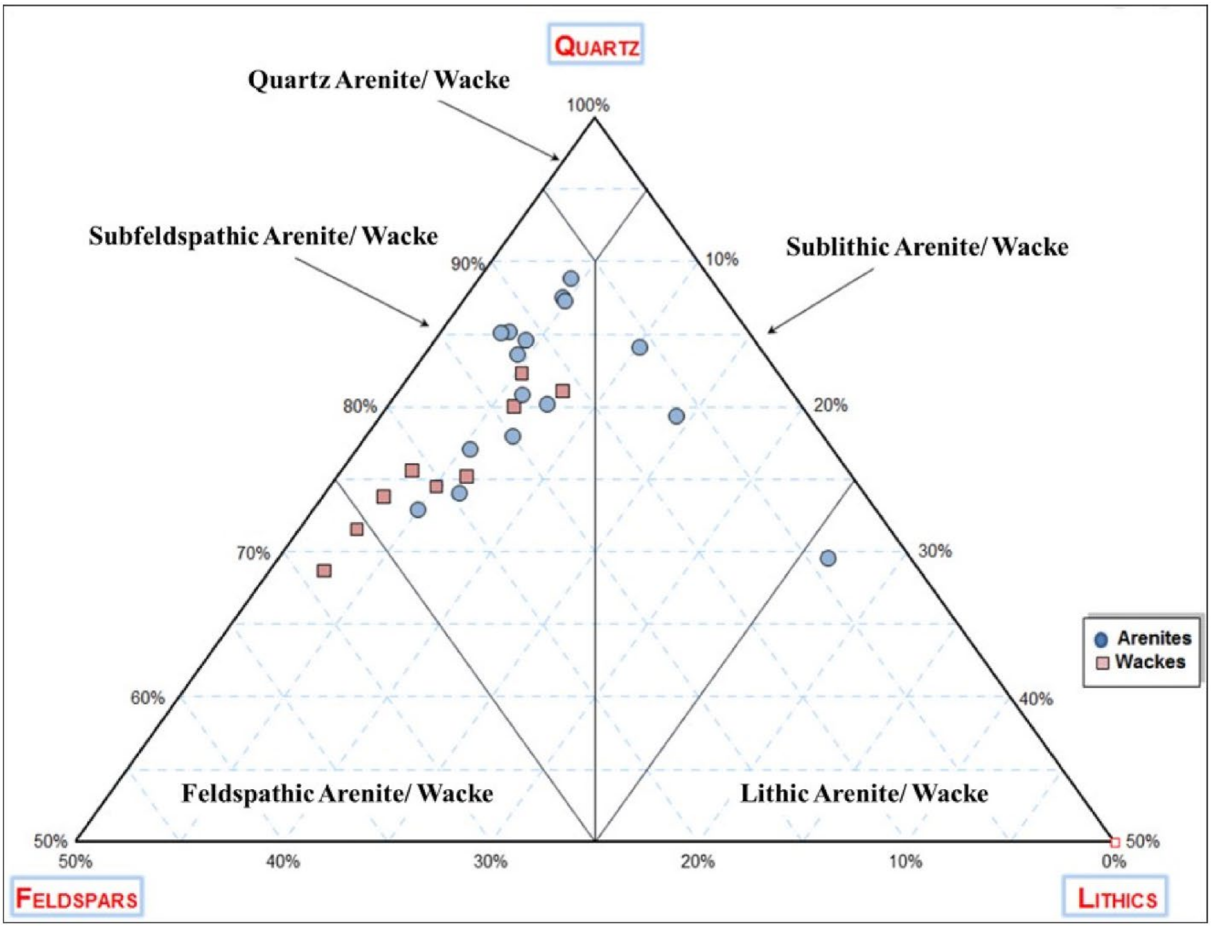

Fig. 6: Ternary plot showing detrital composition of Abu Madi Sandstone of Salma-4 well.

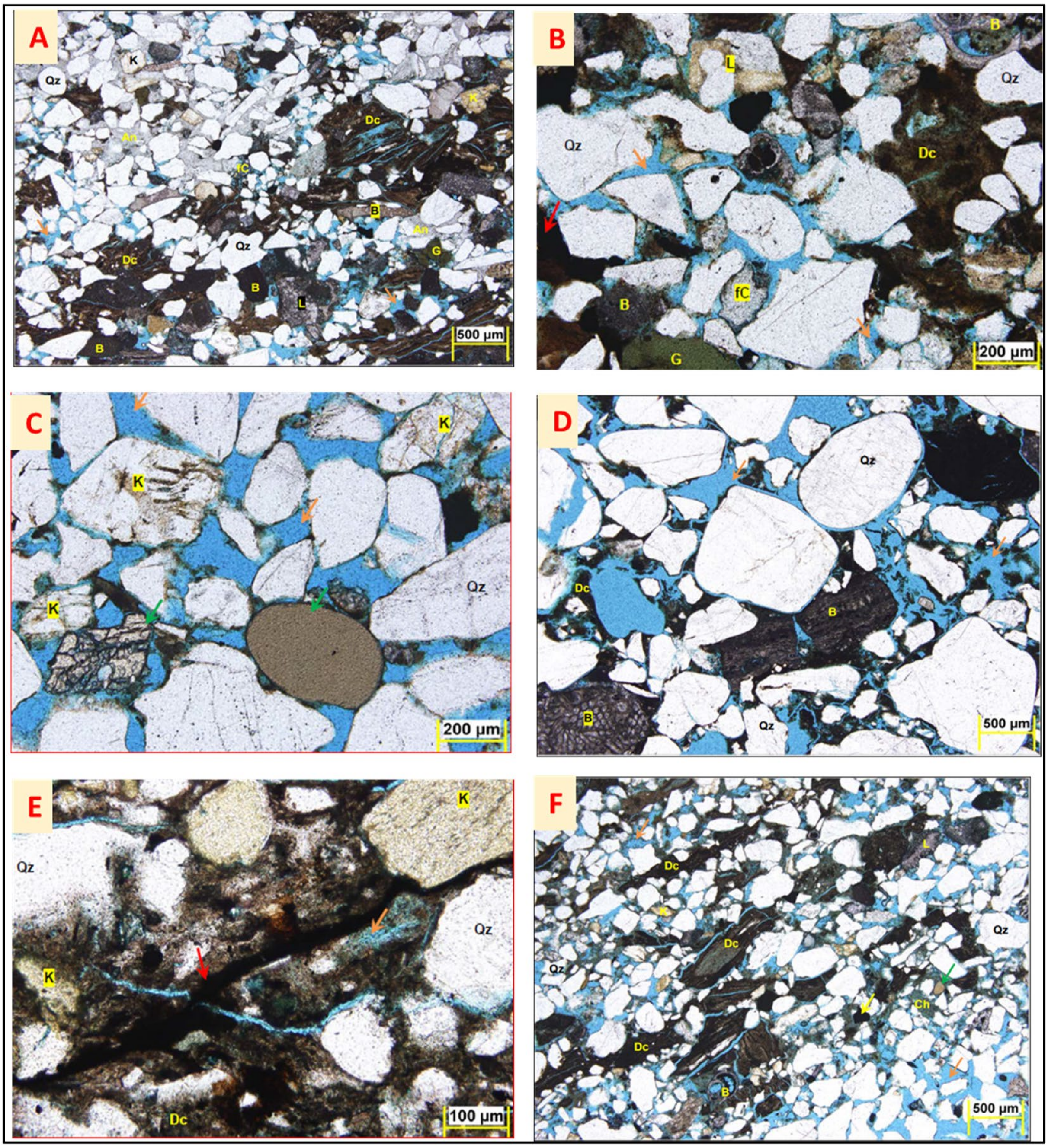

Fig. 7: Thin section microphotographs illustrating different sandstones microfacies of Abu Madi Formation (Mineral symbols: Anhydrite, An; Quartz, Qz ; K-feldspars, K; Glauconite, G ; Bioclasts , B ; Plagioclase feldspars , Ps; Lithic fragments , L ; Detrital clays , Dc ; Porosity (Orange Arrows), Heavy Minerals (Green Arrows), Residual Hydrocarbons (Red Arrows).

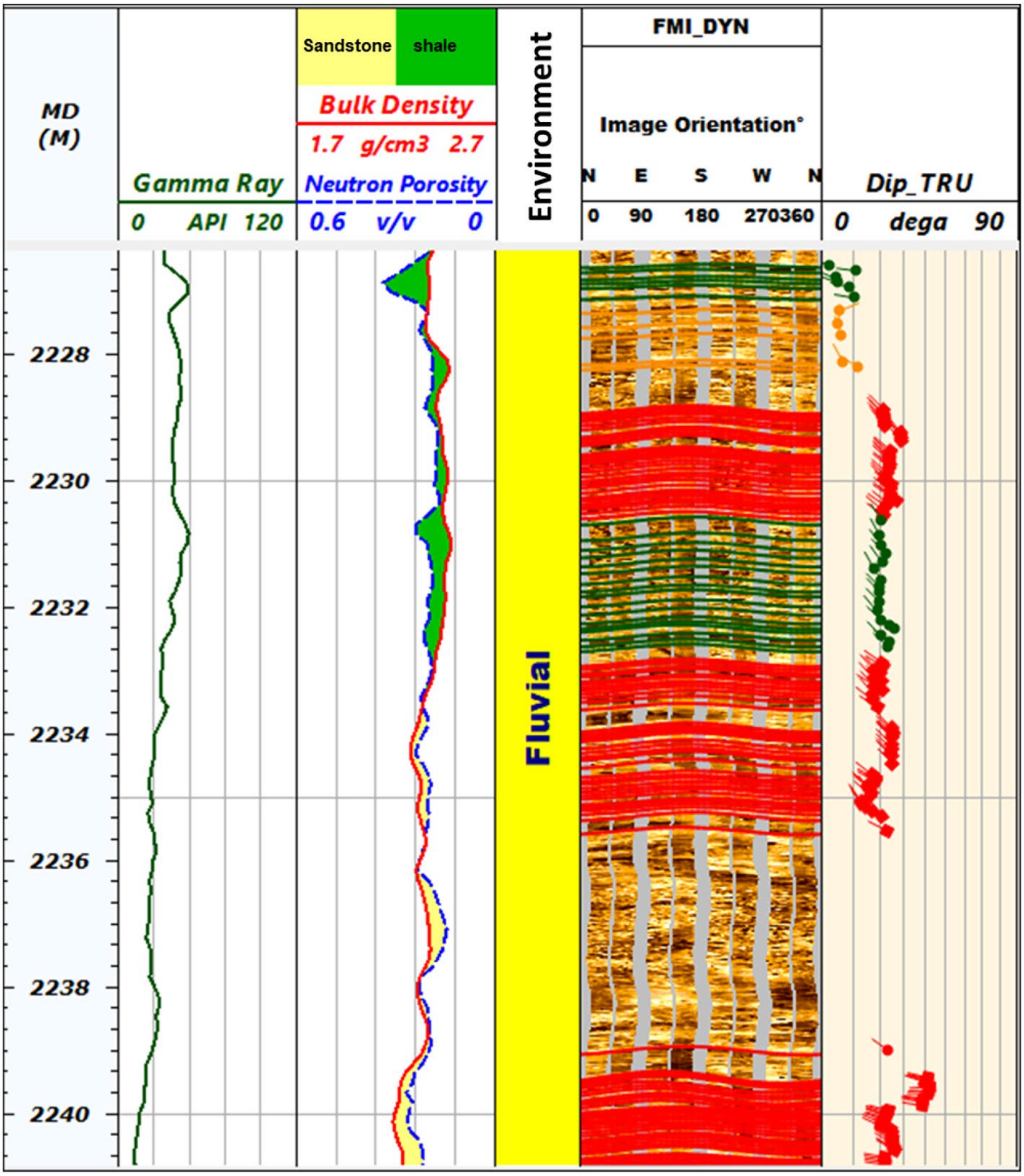

Fig. 8: FMI interpretation showing Abu Madi sedimentary facies (Fluvial channel) in Salma-4 well.

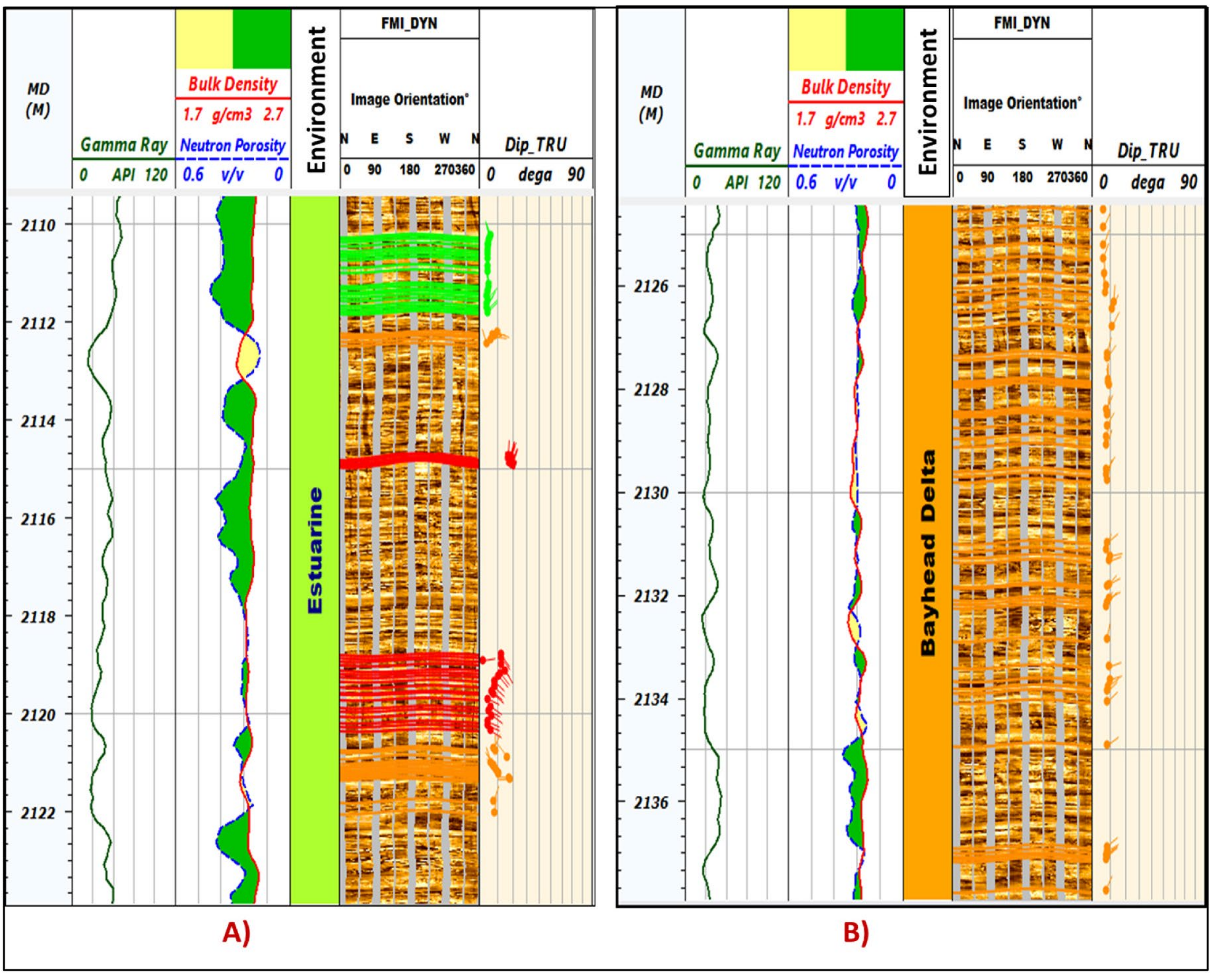

Fig. 9: FMI interpretation showing Abu Madi sedimentary facies (Tidal channel) in Salma-4 well.

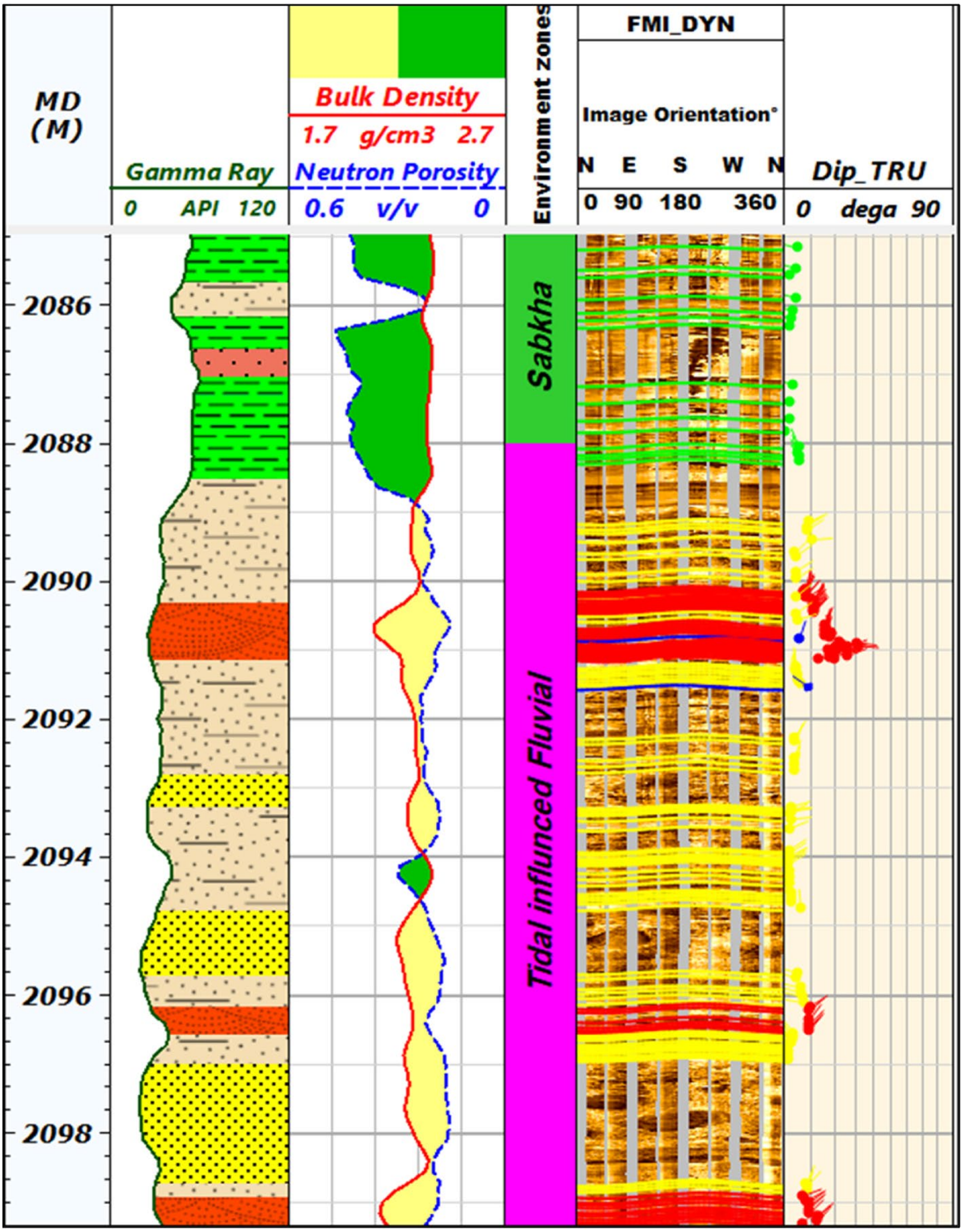

Fig. 10: FMI interpretation showing Abu Madi sedimentary facies (bayhead delta) in Salma-4 well.

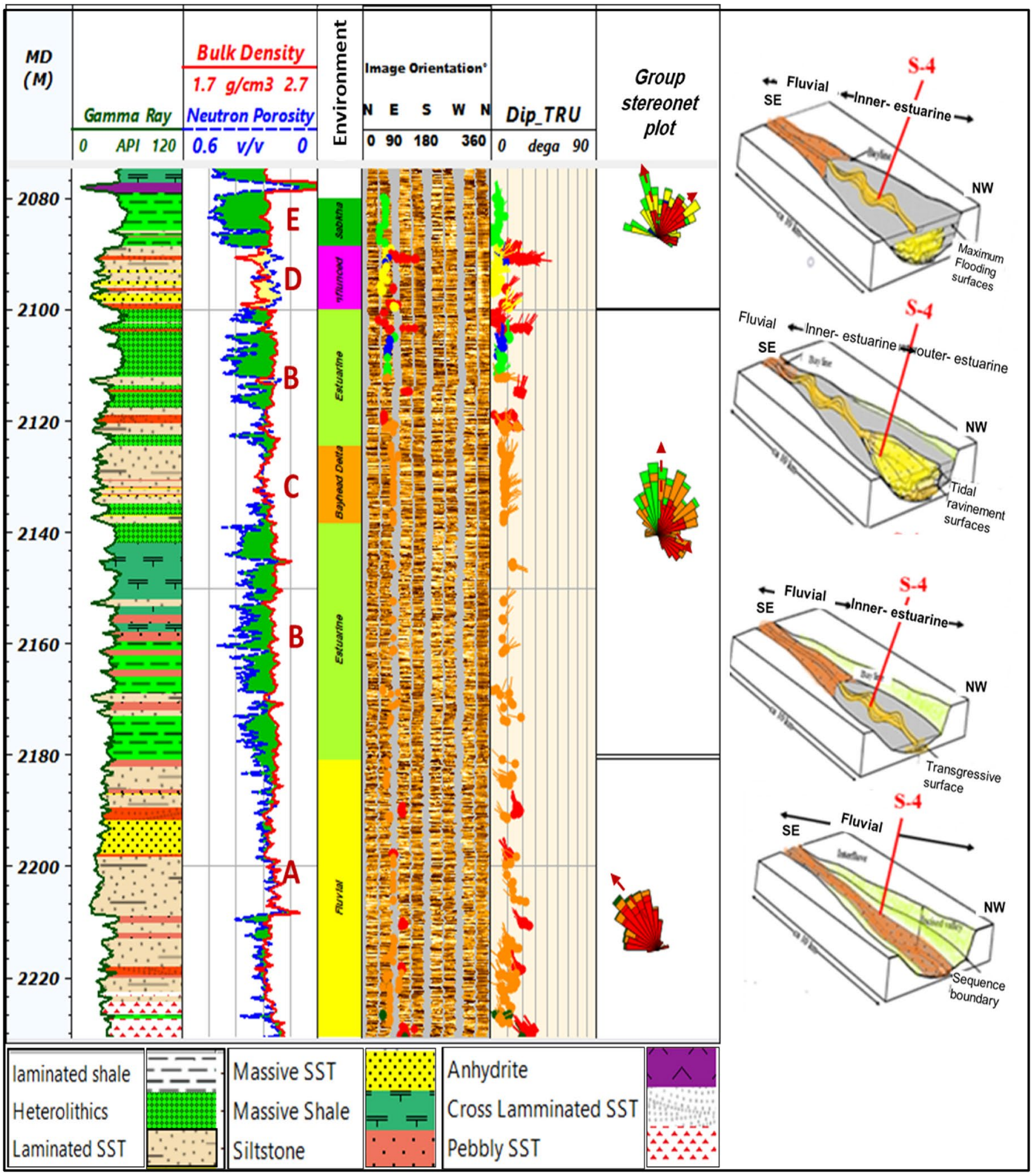

Fig. 11: Composite FMI interpretation showing Abu Madi sedimentary facies and depositional model in Salma-4 well.

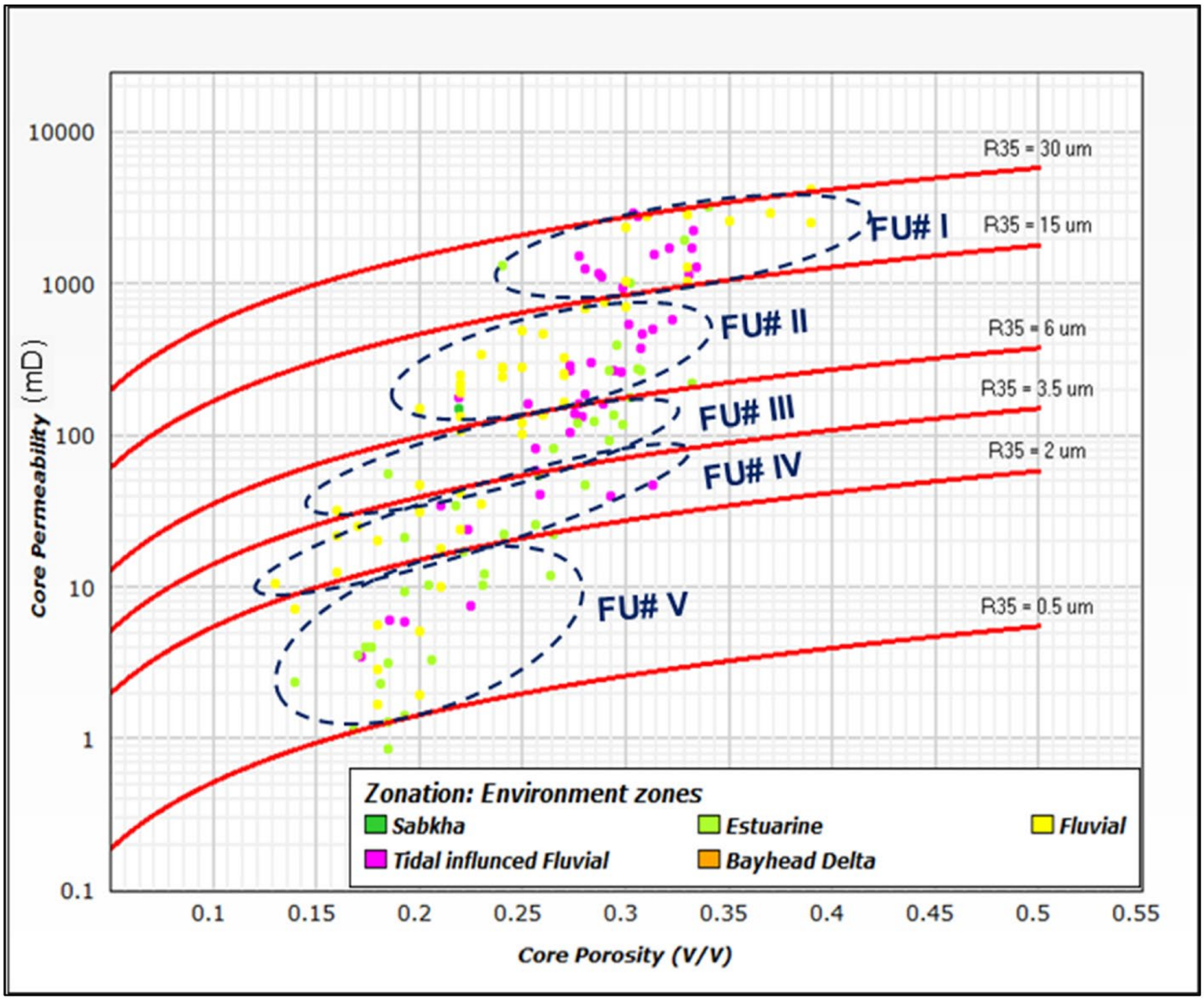

Fig.12: Porosity vs. permeability cross plot for Abu Madi sedimentary facies (The colored lines are R35 pore throat radii).

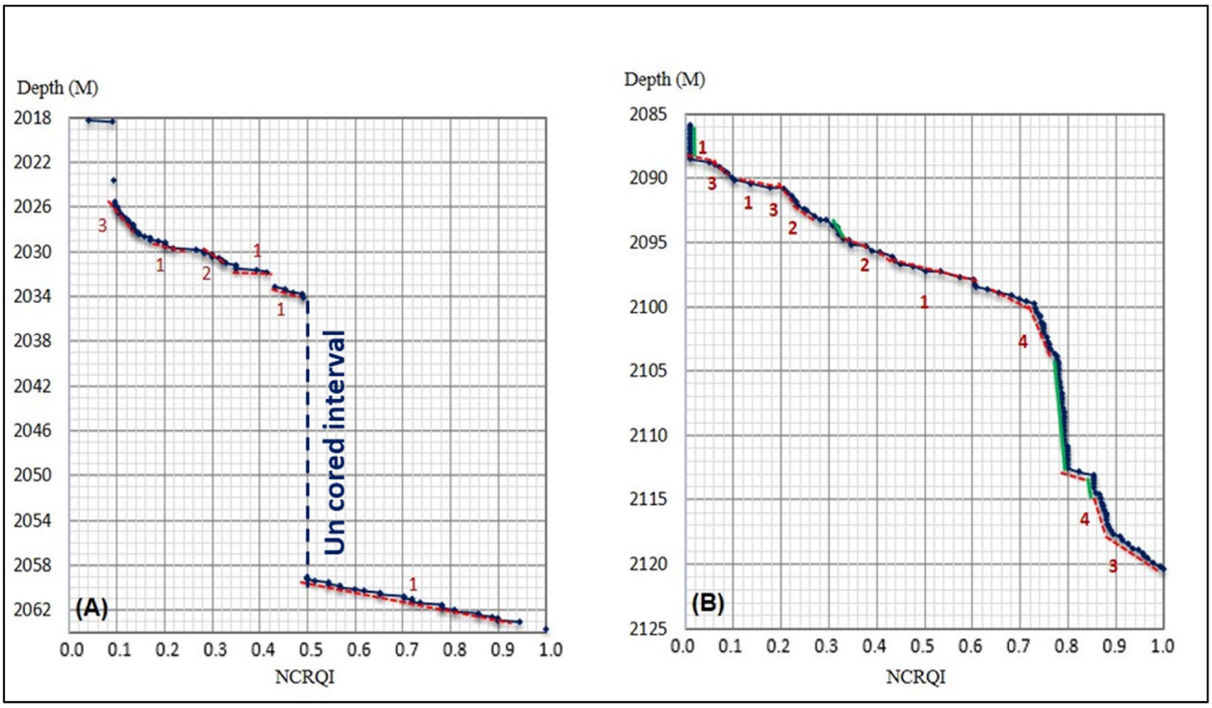

Fig.13: NCRQI – Depth Cross plot for Abu Madi sedimentary facies; (A) Salma-2 well, (B) Salma-4 well.

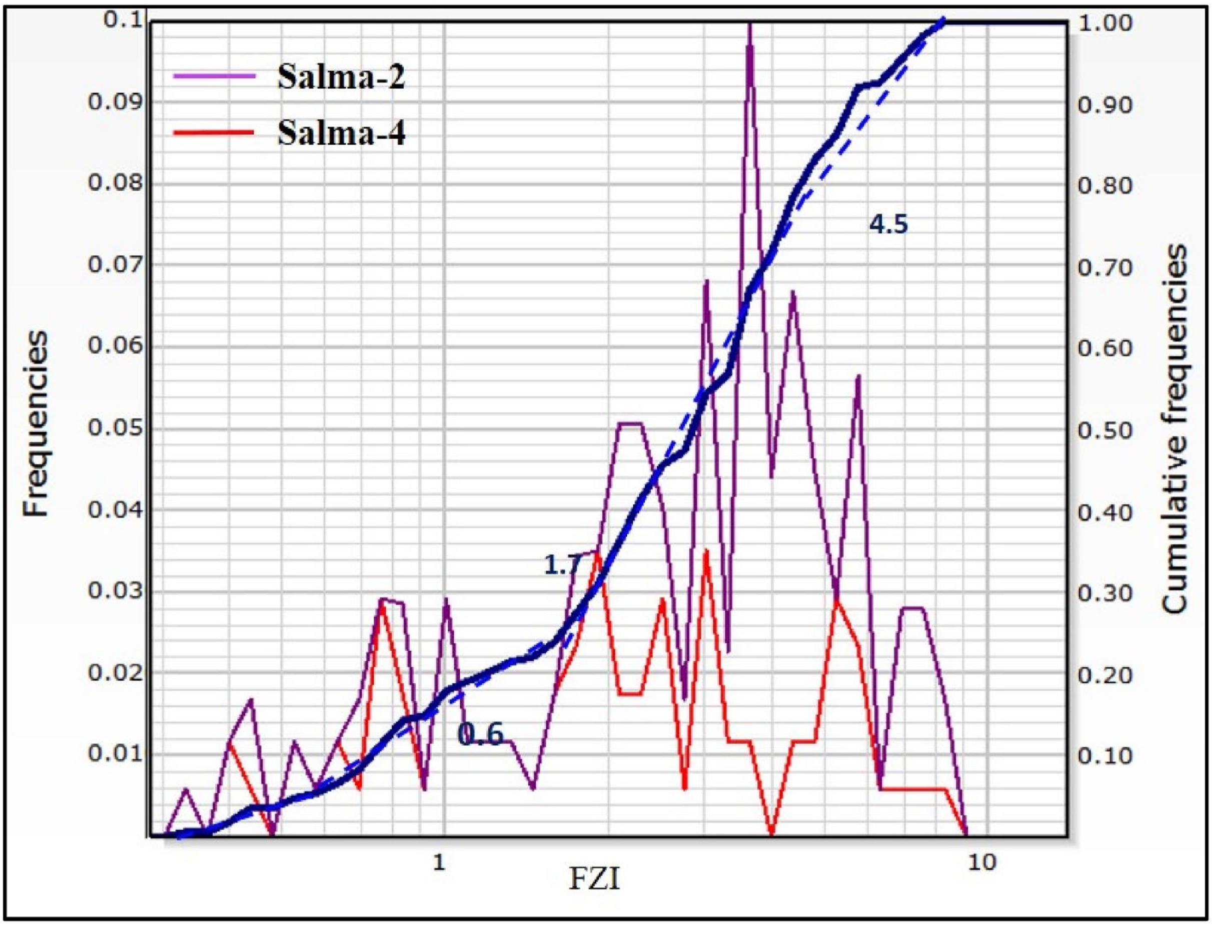

Fig.14: Core FZI distribution and cumulative curves for Abu Madi in Salma-2 and Salma-4 wells.

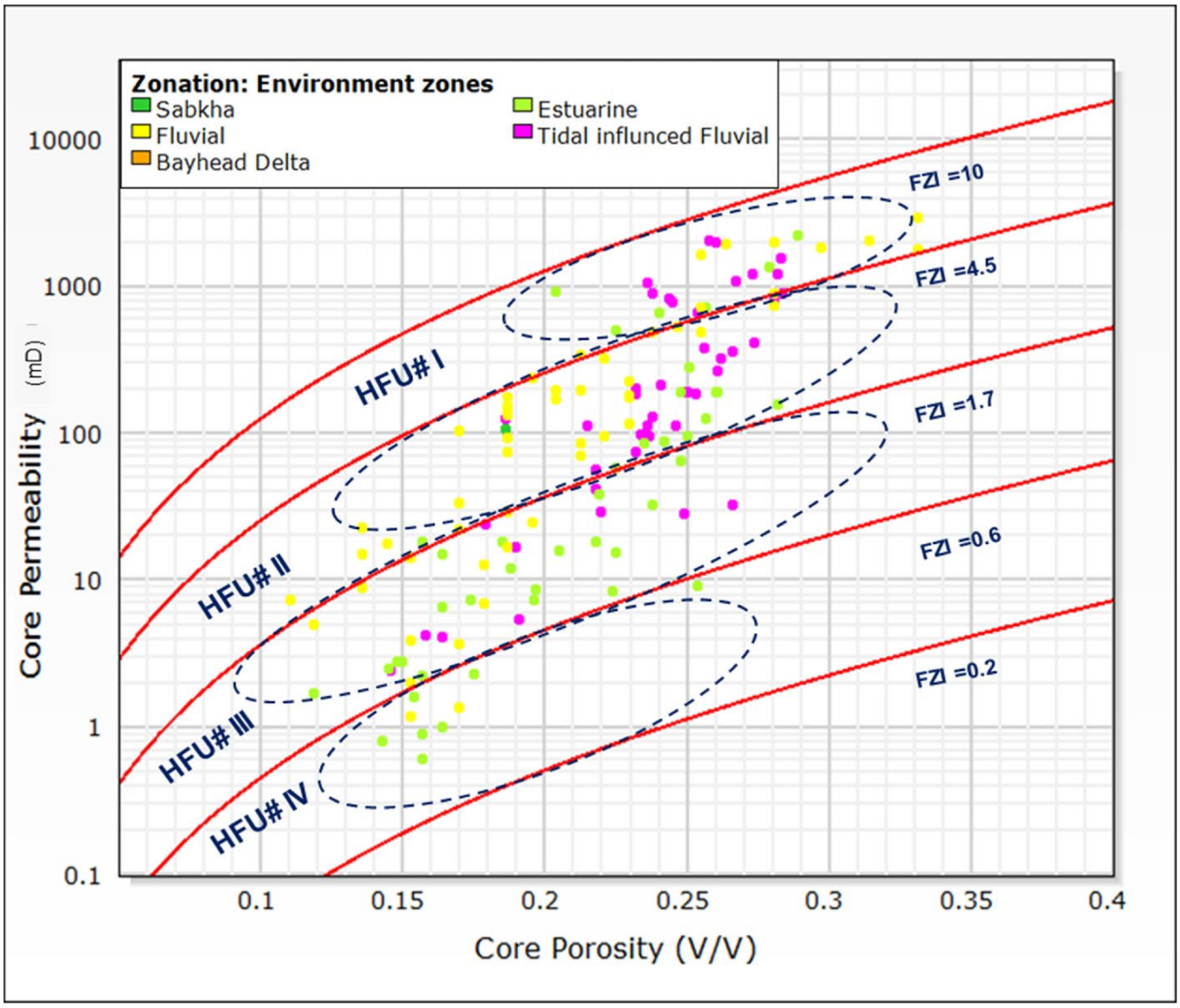

Fig.15: porosity vs. horizontal permeability Cross plot for Hydraulic flow units (HFU) of Abu Madi sedimentary facies.

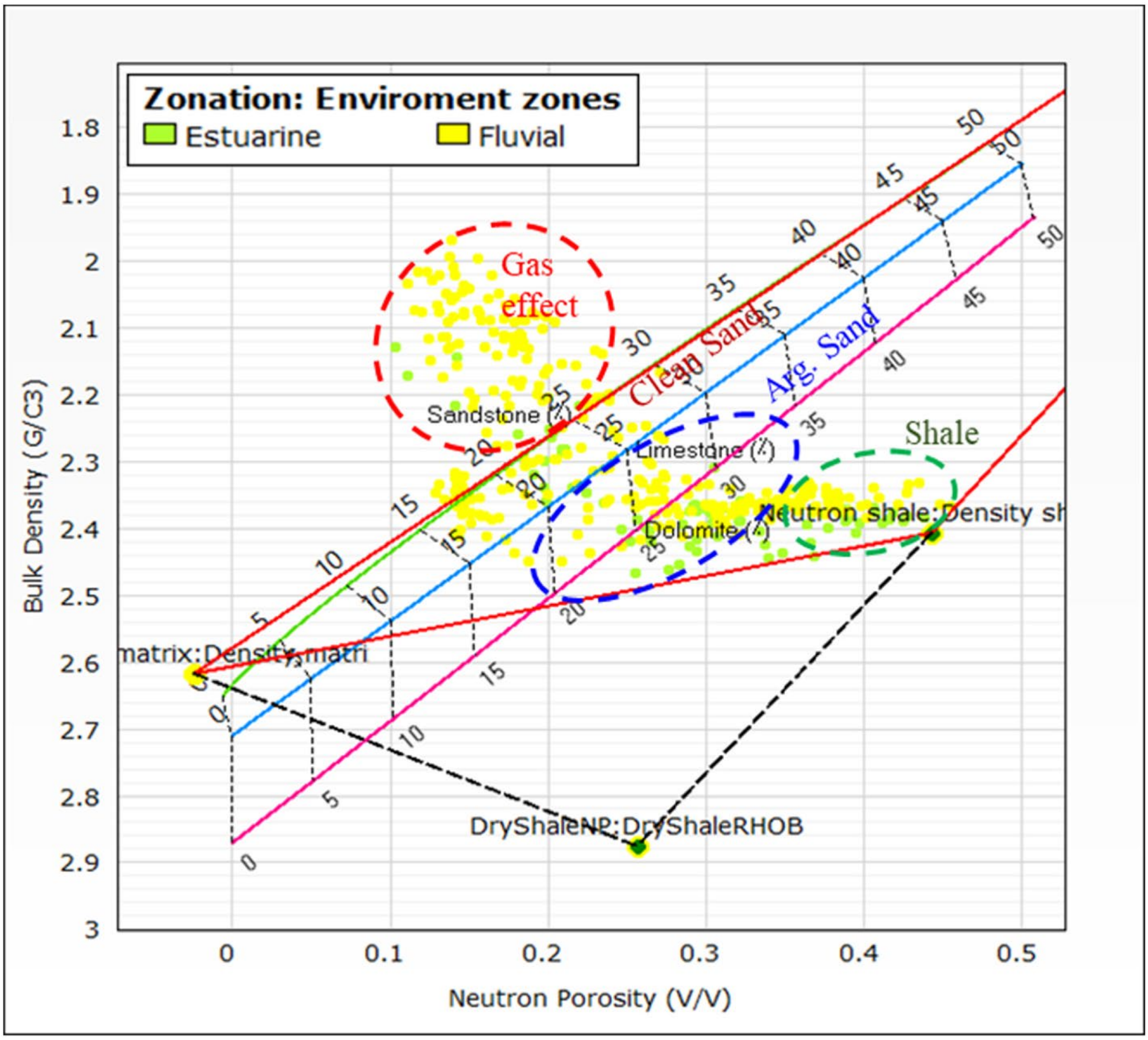

Fig.16: Density- neutron cross plot for Salma-2 well.

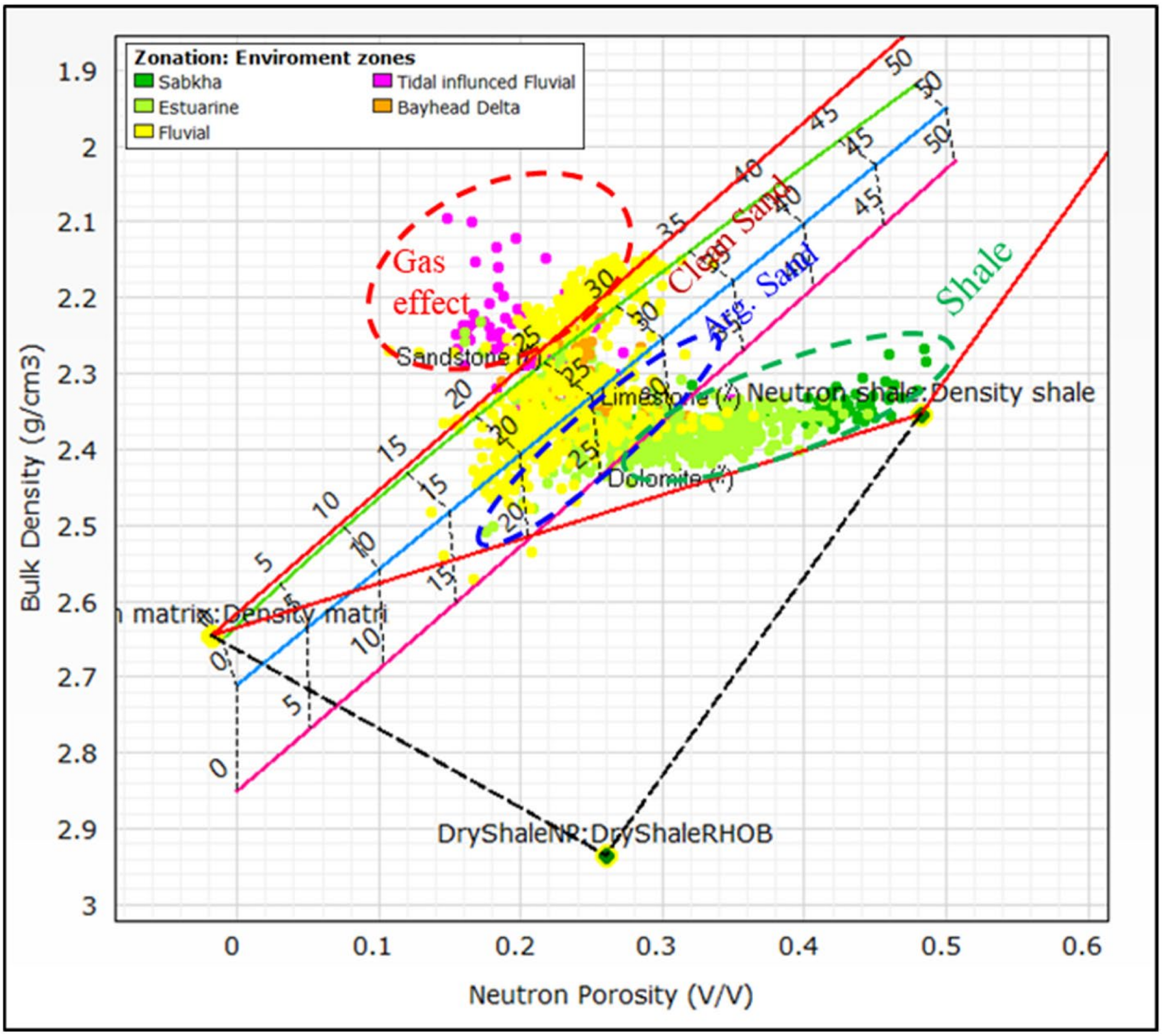

Fig.17: Density- neutron cross plot for Salma-4 well

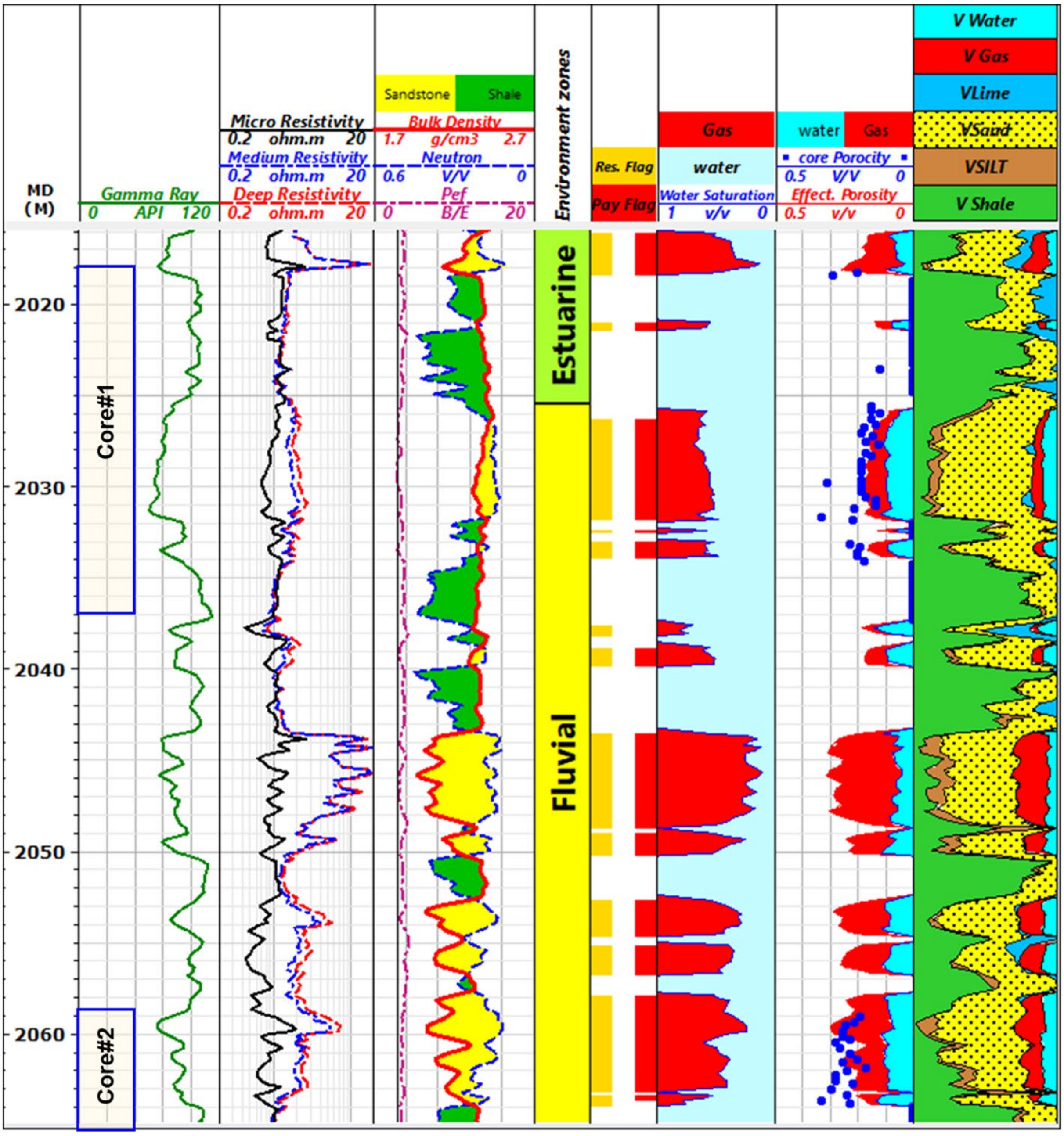

Fig.18: Composite logs showing porosity, water saturation, lithology, and depositional environment for Abu Madi Formation in Salma-2 well.

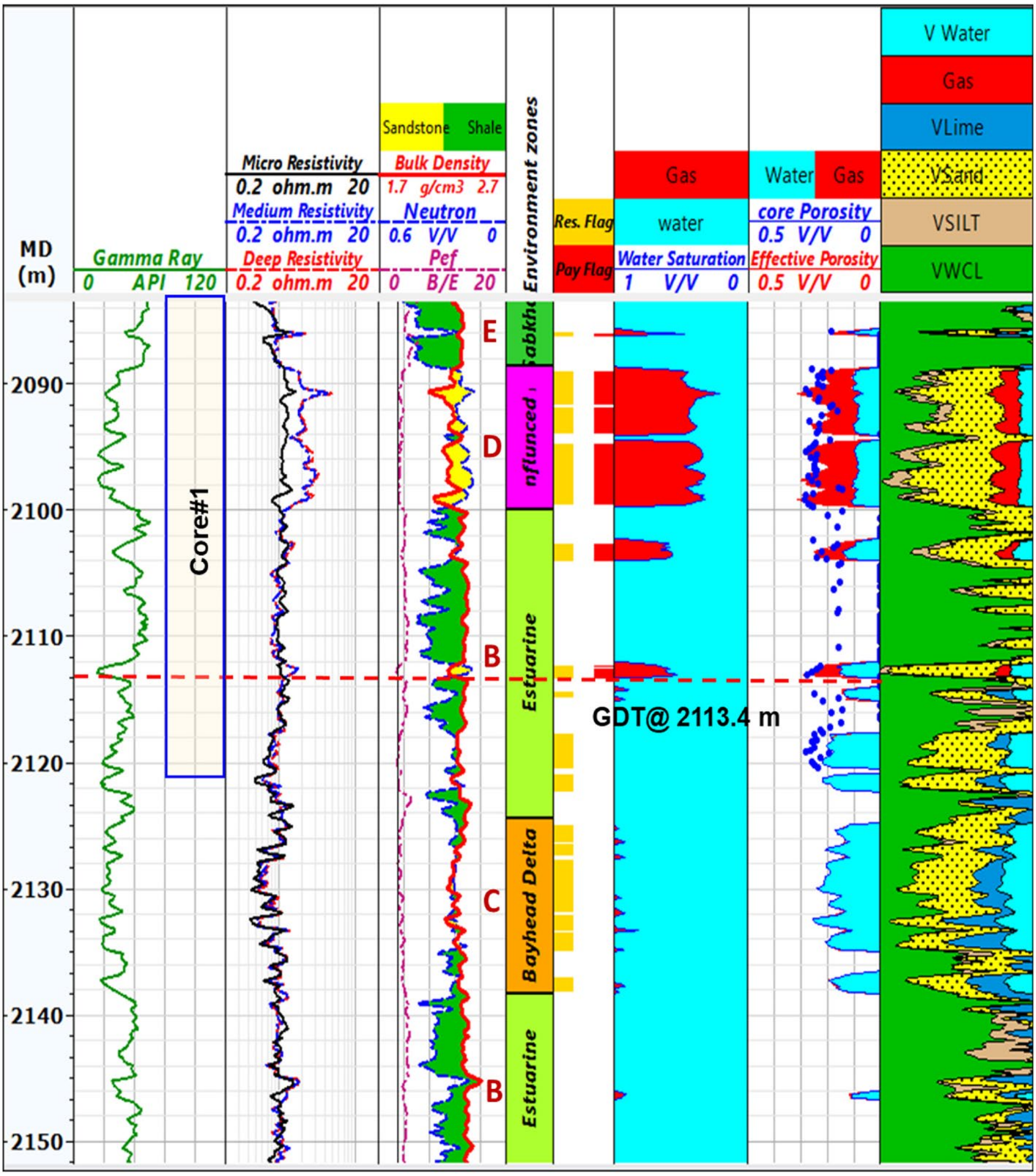

Fig.19: Composite logs showing porosity, water saturation, lithology, and depositional environment for Abu Madi Formation in Salma-4 well.

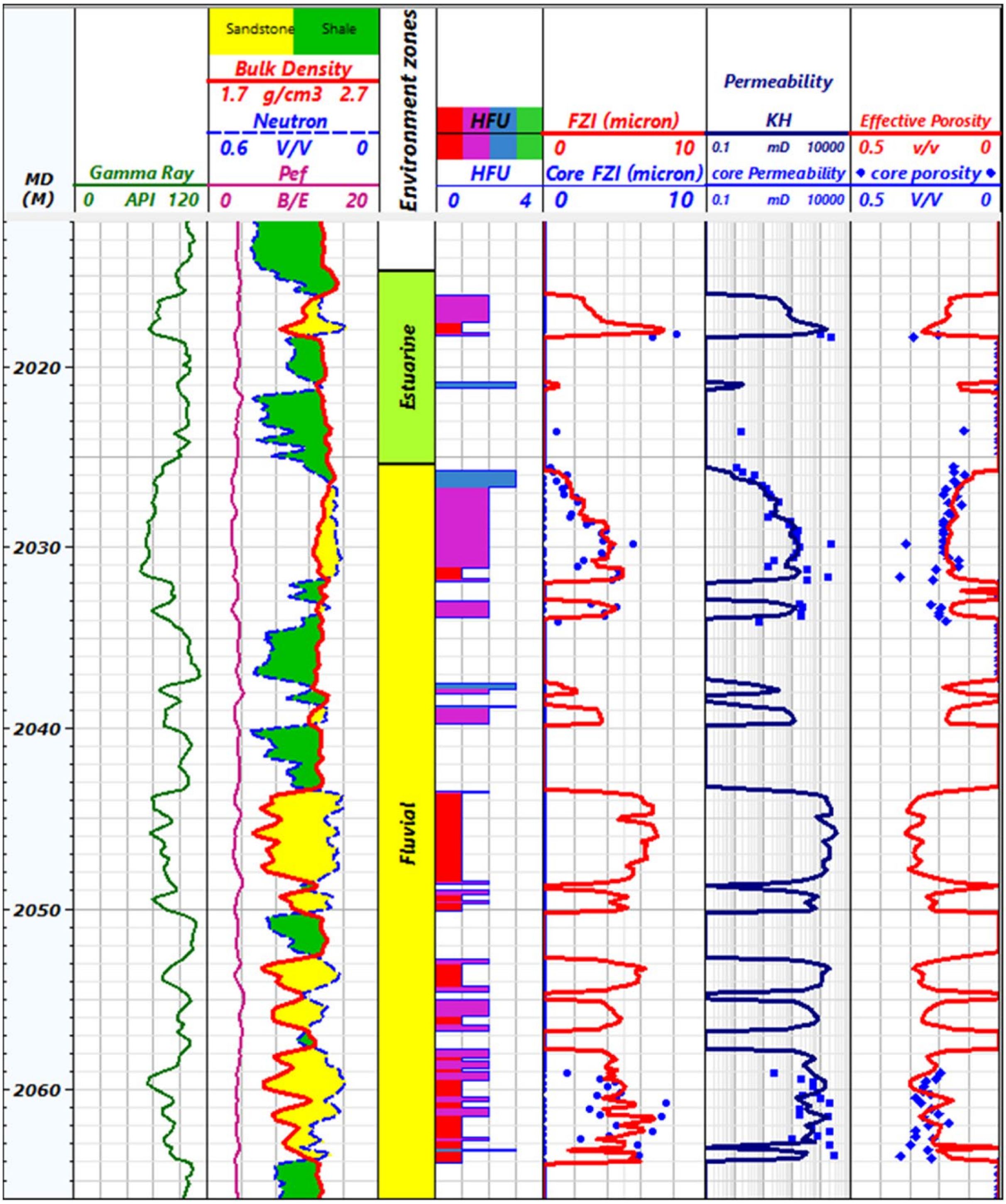

Fig.20: Composite log from neural log showing porosity, permeability, FZI, HFU and depositional environment for Abu Madi Formation in Salma-2 well.

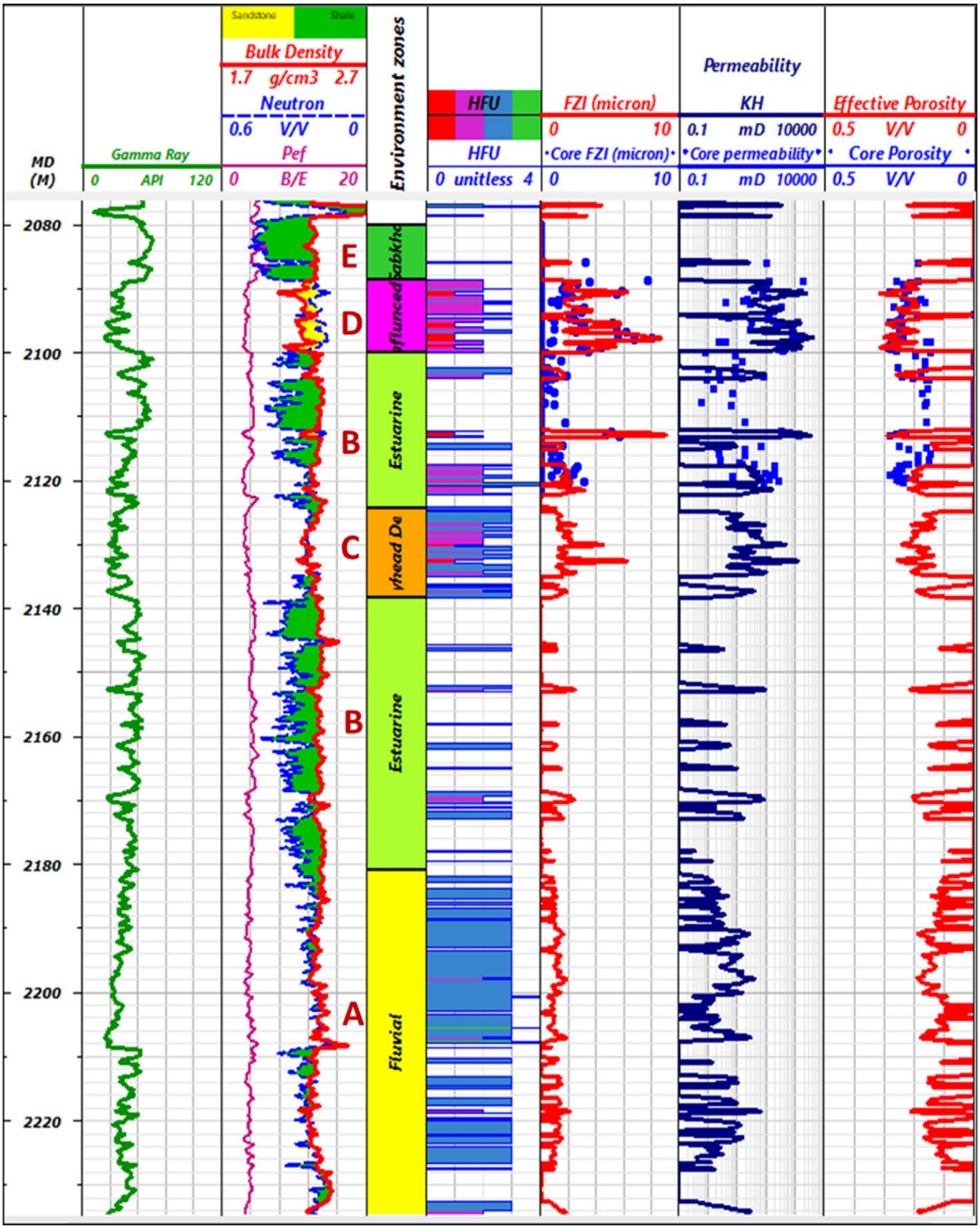

Fig.21: Composite log from neural log showing porosity, permeability, FZI, HFU and depositional environment for Abu Madi Formation in Salma-4 well.

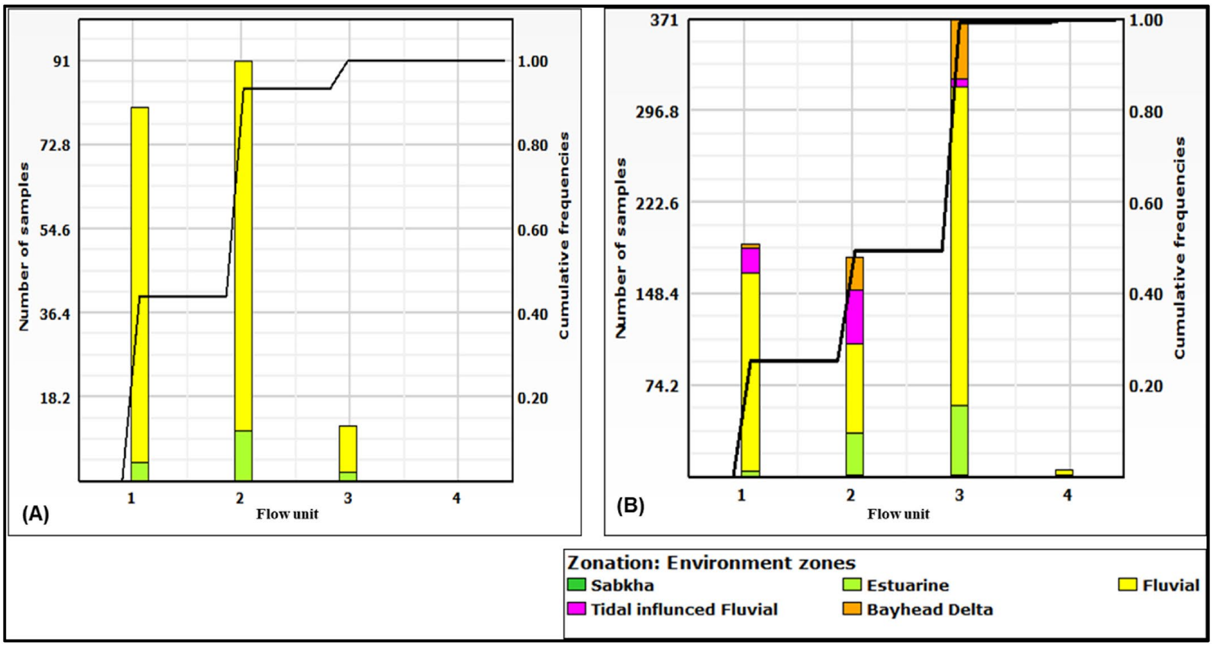

Fig.22: Hydraulic Flow units showing their distributions related to different reservoir units and environment; (A) Salma-2, (B) Salma-4 wells.

1454

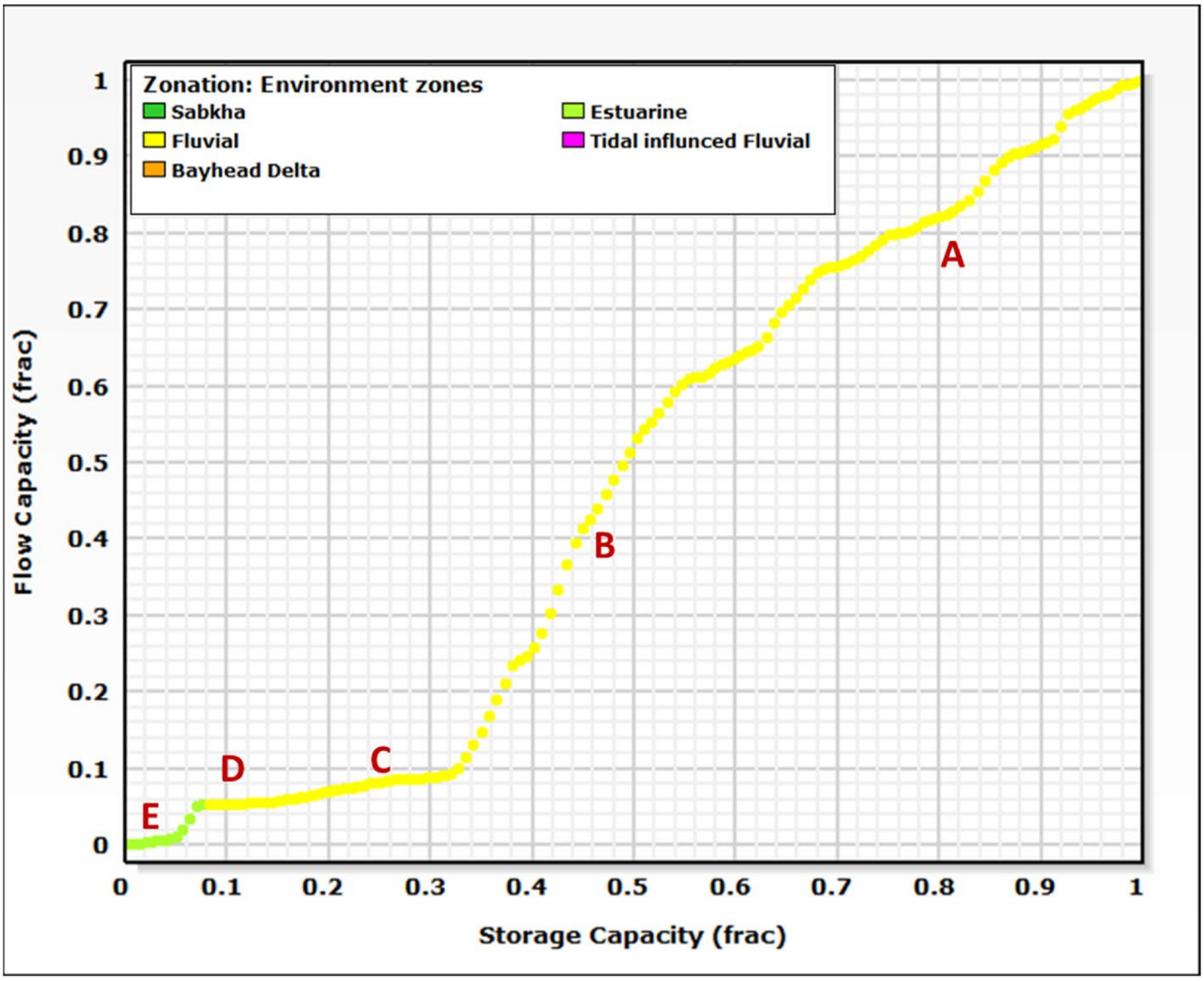

1455 *Fig.23: Stratigraphic modified Lorenz plot (SMLP) for Messinian reservoir in Salma-2 well.*

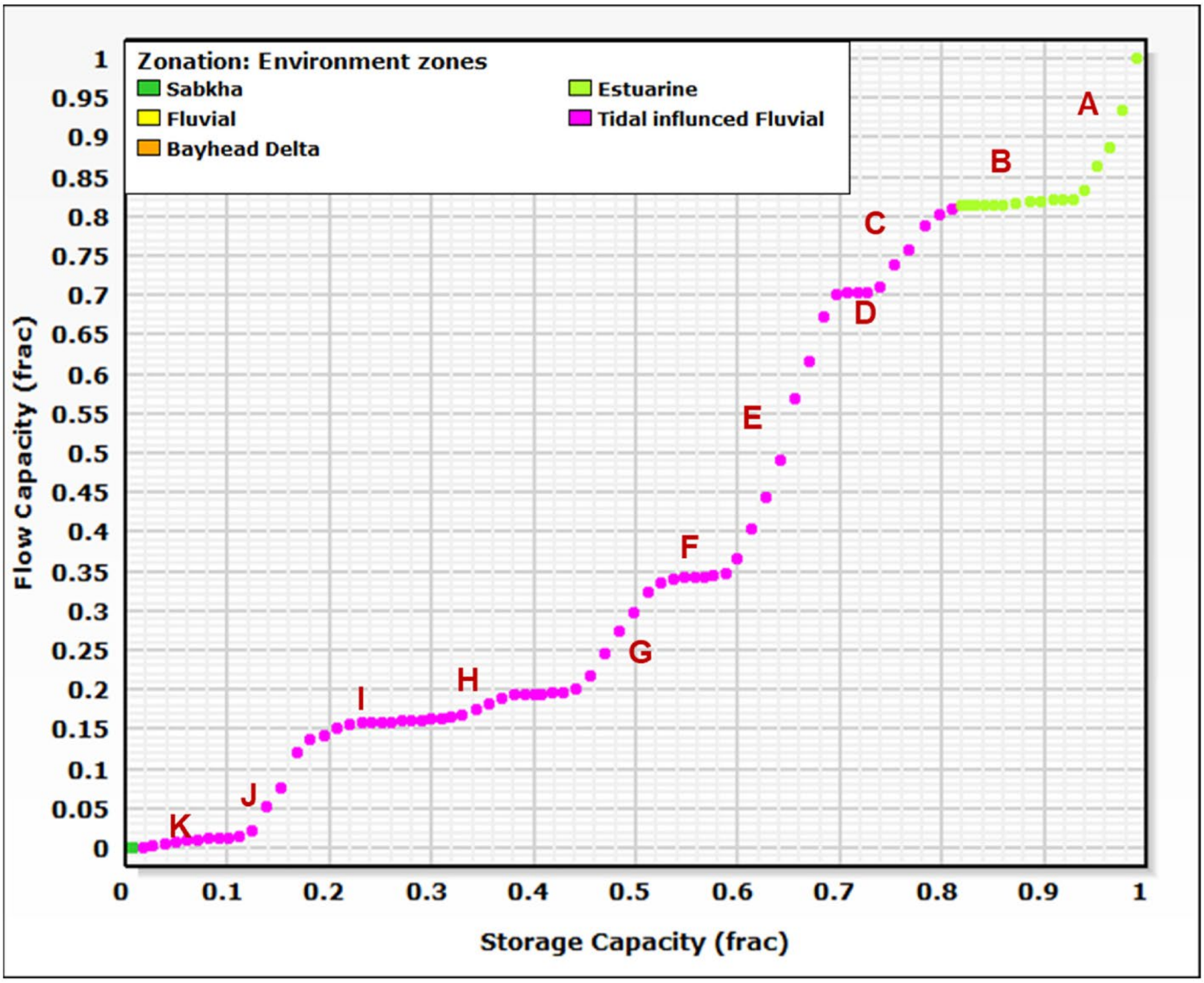

1456

1457 *Fig.24: Stratigraphic modified Lorenz plot (SMLP) for Messinian reservoir in Salma-4 well.*